Title: Cholinergic Modulation Shifts the Response of CA1 Pyramidal Cells to Depolarizing Ramps via TRPM4 Channels with Implications for Place Field Firing

Abbreviated Title: Cholinergic Modulation Shifts the Response of CA1 Pyramidal Cells

Author Names and Affiliations: Crescent Combe[1], Carol Upchurch[2], Carmen C. Canavier[2]* and Sonia Gasparini[1,2]*

[1]Neuroscience Center of Excellence, and [2]Department of Cell Biology and Anatomy, School of Medicine, Louisiana State University Health Sciences Center, New Orleans, Louisiana, USA 70112

* these authors jointly supervised this work

Corresponding author: Sonia Gasparini, Neuroscience Center, Louisiana State University Health Sciences Center, New Orleans, 2020 Gravier St., New Orleans, LA 70112, sgaspa1@lsuhsc.edu

Number of pages: 38

Number of figures: 8

Conflict of interest statement: The authors declare no competing financial interests.

Acknowledgements: This work was funded by NIH R01 MH115832 under the CRCNS program to SG and CCC.

Abstract

A synergistic combination of *in vitro* electrophysiology and multicompartmental modeling of rat CA1 pyramidal neurons identified TRPM4 channels as major drivers of cholinergic modulation of the firing rate during a triangular current ramp, which emulates the elevation in synaptic input received while traversing the place field. In control, fewer spikes at lower frequencies are elicited on the down-ramp compared to the up-ramp. The cholinergic agonist carbachol (CCh) reverses this spike rate adaptation, causing more spikes to be elicited on the down-ramp than the up-ramp. The non-specific TRP antagonist flufenamic acid and the TRPM4-specific blockers CBA and 9-phenanthrol, but not the TRPC-specific antagonist SKF96365, reverse the effect of CCh; this implicates the Ca^{2+}-activated nonspecific cation current, I_{CAN}, carried by TRPM4 channels. Modeling suggests that the IP_3 receptor is the locus that requires both CCh and sustained depolarization to produce the rightward shift in firing rate along the ramp. In the model, a step change in IP_3, representing the activation of muscarinic receptors by CCh, coupled with an increase in bulk [Ca^{2+}] due to voltage-gated Ca^{2+} influx during the ramp, activates Ca^{2+}-induced Ca^{2+} release (CICR). CICR in turn activates TRPM4, via a nanodomain required by the presumed micromolar half-activation for TRPM4.

Introduction

Release of the neuromodulator acetylcholine is thought to be correlated with certain brain states or functions (Pepeu and Giovannini, 2004). In the hippocampal formation, elevated acetylcholine is associated with exploration (Bianchi et al., 2003), particular memory processes (Micheau and Marighetto, 2011), REM sleep (Hutchison and Rathore, 2015), and response to novelty (Acquas et al., 1996; Thiel et al., 1998; Giovannini et al., 2001).

The major cholinergic input to the hippocampus is from the medial septum and diagonal band of Broca, which innervate all hippocampal subfields (Dutar et al., 1995). As for the degree to which acetylcholine release is spatially targeted, this is still under debate (Disney and Higley, 2020; Sarter and Lustig, 2020); however it has been shown that CA1 receives cholinergic afferents in all layers, although at different densities (Nyakas et al., 1987; Aznavour et al., 2002). Pyramidal neurons express G-protein-coupled metabotropic acetylcholine receptors (mAChRs) (Levey et al., 1995), more so than they do ionotropic (nicotinic) receptors, which are primarily on interneurons in this region (Dani and Bertrand, 2007). M_1 mAChRs, in particular, are found on both dendritic shafts and spines of CA1 pyramidal neurons (Yamasaki et al., 2010).

Elevated acetylcholine in the hippocampal formation is thought to favor memory encoding, and modulates theta oscillations (Hasselmo, 2006), which in turn modulate place cell firing (Easton et al., 2012). There is evidence that cholinergic activity regulates long-term synaptic plasticity (Huerta and Lisman, 1995; Palacios-Filardo and Mellor, 2019; Fernández de Sevilla et al., 2021). Cholinergic activation also influences intrinsic properties of neurons, which result in membrane potential depolarization (Brown and Adams, 1980), increase in firing rate (Benardo and Prince, 1982), and modulation of input/output relationships, for example switching from burst to regular firing (Azouz et al., 1994).

In addition to suppressing several potassium currents (Brown and Adams, 1980; Hoffman and Johnston, 1998; Buchanan et al., 2010; Giessel and Sabatini, 2010), cholinergic stimulation has been linked to the activation of a calcium-activated, non-specific cation current, I_{CAN} (Colino and Halliwell, 1993; Egorov et al., 2002; Yoshida et al., 2012). I_{CAN} is attributed to current flowing through channels of the transient receptor potential (TRP) family (Guinamard et al., 2010; Reboreda et al., 2011). The canonical TRP channel, TRPC, has been implicated in cholinergic-mediated persistent firing ((Zhang et al., 2011; Arboit et al., 2020), but see (Egorov et al., 2019)). There is indirect evidence, however, of involvement of TRPM4 channels in the cholinergic activation of I_{CAN}. TRPM4 activation downstream of group I metabotropic glutamate receptors in pre-Botzinger cells (Mironov, 2008), implicates the $G_{q/11}$ pathway shared by $mGluR_{1/5}$ and mAChR $M_{1/3/5}$. In HEK cells transfected with TRPM4 cDNA, and in cardiac myocytes, activation of TRPM4 channels is secondary IP3 receptor activation (Launay et al., 2002; Gonzales et al., 2010; Gonzales and Earley, 2012). Our proposed pathway for cholinergic activation of TRPM4 follows IP_3 activation of IP_3R on the endoplasmic reticulum and subsequent Ca^{2+} release, at a high enough

concentration to activate TRPM4 channels. This requires close apposition of IP_3R and TRPM4, which has been demonstrated to be < 40 nm in smooth muscle (Provence et al., 2017). Although TRPM4 channels are known to be expressed in the soma and apical dendrites of CA1 pyramidal dendrites (Riquelme et al., 2021), their known functions in these neurons are currently limited to a minor role in the afterdepolarization following action potential trains (Lei et al., 2014) and involvement in NMDA-mediated LTP (Menigoz et al., 2016).

Previously, we found that when triangular shaped current ramps intended to emulate the depolarizing input received by a place cell during a place field traversal (Epsztein et al., 2011) were injected at the soma or dendrites of CA1 pyramidal neurons, they elicit fewer spikes on the down-ramp than on the up-ramp (Upchurch et al., 2022). In the current study, we investigated the effect of cholinergic modulation on this firing pattern *in vitro* (slice electrophysiology) and *in silico* (multi-compartmental NEURON model). We found that, at comparable maximum firing rates, cholinergic activation shifts firing to the latter half of the ramp. This shift is blocked by antagonists specific for TRPM4 or intracellular Ca^{2+} buffering. Both CCh and sustained depolarization are required to produce the rightward shift in firing rate along the ramp; the IP_3 receptor is the putative locus for this convergence. Indeed, modeling revealed that the following scenario is likely responsible for the shift: a step change in IP_3 concentration, coupled with an increase in bulk $[Ca^{2+}]_i$ through voltage-gated Ca^{2+} channels due to the depolarizing ramp, activates Ca^{2+}-induced Ca^{2+} release, which in turn activates TRPM4, via a nanodomain. The presence of a nanodomain is required by the presumed micromolar half-activation for TRPM4 (Nilius et al., 2004).

Results

Asymmetric firing on symmetric ramps can be modulated by cholinergic activation

We have previously used triangular-shaped current ramps (Upchurch et al., 2022) to emulate the depolarizing input received by a place cell during a place field traversal (Epsztein et al., 2011), adjusting the amplitude of the ramps for each cell and condition to produce peak frequencies between 10 and 25 Hz as observed in place cells *in vivo* (Hargreaves et al., 2007; Resnik et al., 2012; Bittner et al., 2015). Regardless of whether these ramps are injected at the soma or in the dendrites of CA1 pyramidal neurons, they elicit fewer spikes on the down-ramp than on the up-ramp, due to adaptation mediated by long-term sodium channel inactivation (Fernandez and White, 2010; Venkatesan et al., 2014; Upchurch et al., 2022). Place cell firing is modulated by experience such that the center of the place field shifts in a direction opposite the direction of motion as the environment becomes more familiar (Mehta et al., 1997). This modulation is strongest when animals are first introduced to a novel environment (Roth et al., 2012), suggesting involvement of a novelty signal. Since elevated acetylcholine is thought to be such a signal

(Acquas et al., 1996; Giovannini et al., 2001), we investigated the effect of cholinergic neuromodulation on this firing rate adaptation (Figure 1). Figure 1A1 and 1D1 show typical voltage responses under control conditions to two second-long symmetric ramps injected in the soma or dendrites (approximately 200 μm from soma). This type of response results in a positive value for the normalized difference between spikes fired on the up-ramp versus the down-ramp (we call this an adaptation index, see Methods for definition). A positive index means that neurons fire more on the up-ramp than the down-ramp, whereas a negative value implies the converse. Application of the cholinergic agonist carbachol (CCh, 2 μM) shifts the majority of the action potentials to the down-ramp (Figure 1B1 and 1E1), which results in a decreased value of the index that is negative for most cells, as shown in the scatter plot of group data (Figure 1C and 1F). This shift is significant for short (2 s) ramps in the soma (control 0.33 ± 0.02, CCh -0.25 ± 0.03; $t(20) = 16.741$; $p < 0.0005$; $n = 21$), long (10 s) ramps in the soma (control 0.24 ± 0.02, CCh -0.33 ± 0.06; $t(18) = 9.854$; $p < 0.0005$; $n = 19$), as well as for short and long ramps in the dendrites (2 s ramps: control 0.49 ± 0.04, CCh -0.45 ± 0.07; $t(18) = 12.529$; $p < 0.0005$; $n = 19$; 10 s ramps: control 0.37 ± 0.02, CCh -0.16 ± 0.06; $t(9) = 10.582$; $p < 0.0005$; $n = 10$). Plots of instantaneous frequency versus current injection that correspond to the example voltage responses are shown in Figure 1A2, 1B2, 1D2 and 1E2. In control, frequencies are higher on the up-ramp, while in CCh peak firing is not reached until after the peak current injection. These results demonstrate that cholinergic activity shifts action potential firing to later times during the ramp. The level of cholinergic modulation could therefore be a source of rapid modification of the timing of place cell firing relative to position in the place field.

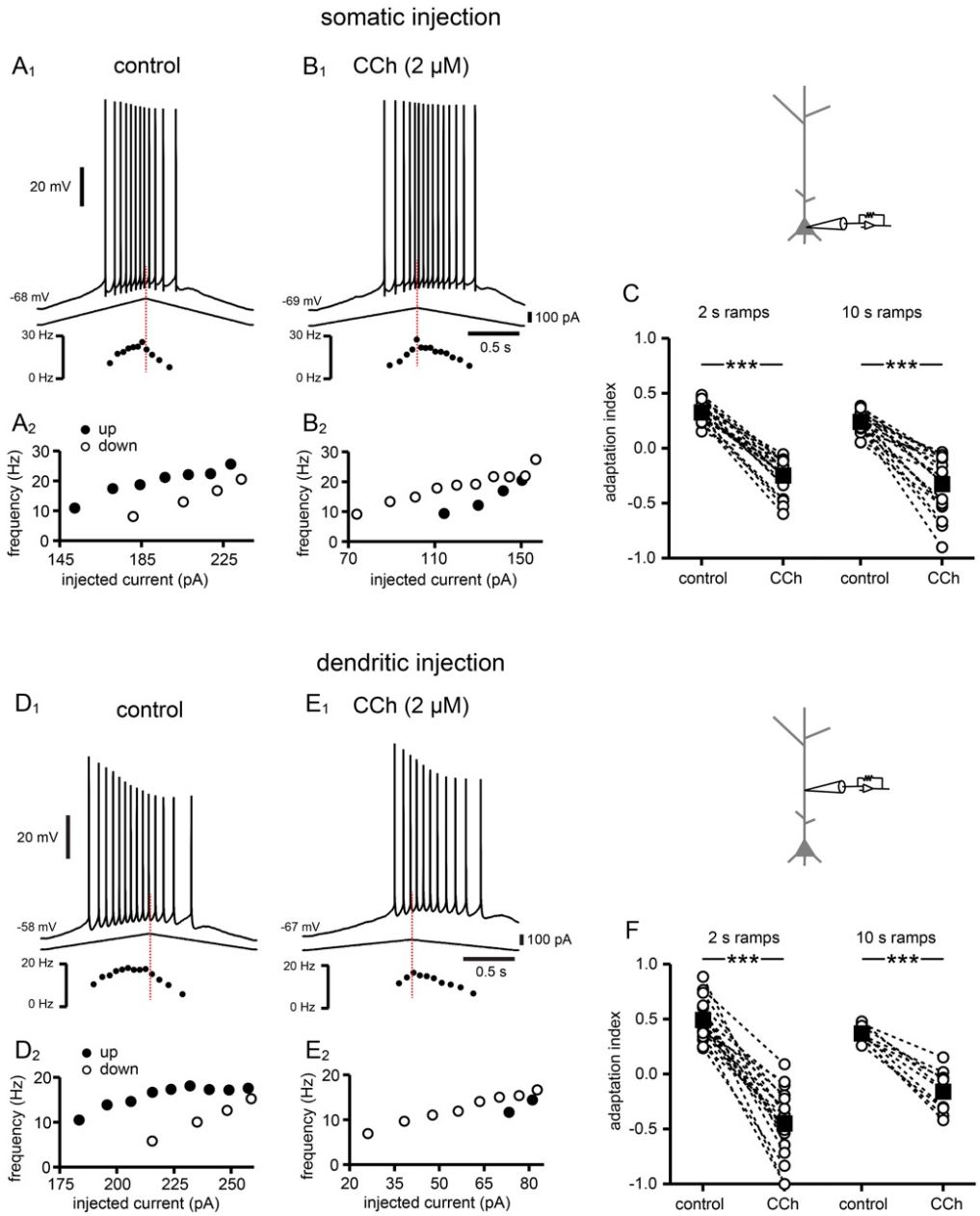

Figure 1. Asymmetric responses to depolarizing current ramps are modulated by carbachol.
A. Somatic injection, control. A1. Voltage trace recorded in the soma for a two second triangular current ramp injected in the soma. Current trace is just below voltage trace. Below current trace is the instantaneous frequency as it changes along the ramp. Red dotted line marks the middle of the ramp. A2. Instantaneous frequency for example in A1, as it changes with injected current. Filled circles, firing on the up-ramp. Open circles, firing on the down-ramp. B. Somatic injection, carbachol. B1 and B2. Same as A1 and A2, but after superfusion with 2 μM CCh. A and B are the same cell. C. Summary data of the adaptation index for somatic ramps, before and after CCh, for two second ramps (n = 21) and ten second ramps (n= 19). Open circles connected by dashed lines represent indices for individual cells, before and after CCh. Black squares with error bars represent group averages ± SEM. In control, all adaptation indices are positive, indicating more action potentials on the up-ramp. In CCh, most adaptation indices are negative, indicating more action potentials on the down-ramp. D. Dendritic injection, control. D1. Voltage trace recorded in the dendrite for a two second triangular current ramp injected in the dendrite, approximately 200 μm from the soma. Current traces and instantaneous frequency plots are just below voltage trace and red dotted line marks the middle of the ramp. D2. Instantaneous frequency for example in D1, as it changes with injected current. Filled circles represent firing on the up-ramp. Open circles represent firing on the down-ramp. E. Dendritic injection, carbachol. E1 and E2. Same as D1 and D2, but after superfusion with 2 μM CCh. D and E are from the same cell. F. Summary data of the adaptation index for dendritic ramps, before and after CCh, for two second ramps (n = 19) and ten second ramps (n= 10). Positive and negative adaptation indices have the same meaning as in C. *** $p < 0.0005$.

Carbachol is often used to more easily study cholinergic signaling in biological tissues, because it is not susceptible to hydrolysis by acetylcholinesterase, which is preserved and active in hippocampal slices (Avignone and Cherubini, 1999). To verify that the effects of the endogenous neuromodulator were comparable to those of its synthetic analog, we repeated the experiments in Figure 1 with different concentrations of acetylcholine. Like carbachol, acetylcholine shifted the firing response to the right on the ramp, albeit to a more moderate degree (Figure 2A-D). A one-way repeated measures ANOVA was carried out to determine if there was an effect on the adaptation index of three concentrations of ACh within the same neurons. The assumption of sphericity was violated, so a Greenhouse-Geisser correction was applied ($\varepsilon = 0.574$). There was a significant effect of ACh on the adaptation index, plotted in Figure 2E (control 0.35 ± 0.04; 2 μM ACh 0.14 ± 0.04; 10 μM ACh 0.00 ± 0.06; 15 μM ACh -0.02 ± 0.06; $F(1.722, 20.665) = 44.360$; $p < 0.0005$, $n = 13$). Bonferroni-adjusted post hoc tests demonstrated significant differences between the control condition and all concentrations of ACh (all comparisons $p < 0.0005$), and between the lowest concentration and the subsequent higher concentrations (for 2 μM compared to 10 μM, $p = 0.001$; for 2 μM compared to 15 μM, $p = 0.01$). There was not a significant difference between 10 μM and 15 μM ACh. Due to likely degradation via acetylcholinesterase, we speculate that the actual concentration in the slices is lower than the applied one. CCh is not susceptible to degradation by acetylcholinesterase and its concentration, which in our experiments is markedly lower than that used in many experiments on cholinergic modulation of neuronal activity (Bland et al., 1988; Fisahn et al., 1998; Knauer et al., 2013), is therefore more consistent, which may explain the more pronounced shift in spiking in Figure 1 as compared to Figure 2. Nonetheless, our results with ACh suggest that there are concentration-dependent effects of the endogenous neuromodulator on firing rate adaptation. This could have implications regarding ACh fluctuations for a place cell's firing within its place field.

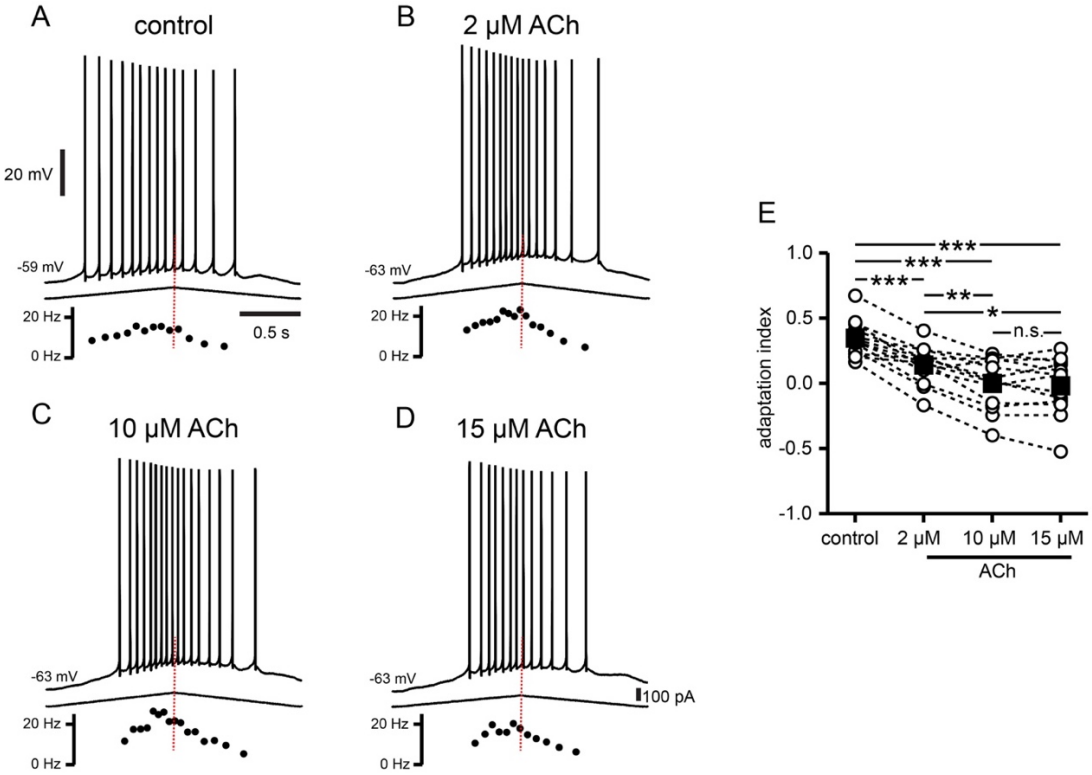

Figure 2. Modulation by acetylcholine of response to symmetric ramps is concentration dependent.
A. Voltage traces recorded in the soma for a two second triangular current ramp injected in the soma in control. Current traces and instantaneous frequency plots are just below voltage traces. Red dotted line marks the middle of the ramp. B-D. Same as A, after superfusion with 2 μM ACh (B), 10 μM ACh (C), and 15 μM ACh (D). A through D are from the same cell. E. Summary data of the adaptation index for control and the three concentrations of ACh, applied in order of increasing concentration (n = 13). Open circles connected by dashed lines represent indices for individual cells over all four conditions. Black squares with error bars represent group averages ± SEM. *** $p < 0.0005$, ** $p = 0.001$, * $p = 0.01$.

Cholinergic-associated shift in the timing of firing during the ramp is mediated by TRP channels

An increase in firing on the down-ramp compared to the up-ramp induced by cholinergic activation could result from 1) a decrease in an outward current and/or 2) an increase in an inward current. The cascade of events that follow cholinergic activation in these neurons includes the suppression of a number of outward currents (Brown and Adams, 1980; Hoffman and Johnston, 1998; Buchanan et al., 2010; Giessel and Sabatini, 2010) some of which are also involved in firing rate adaptation (Stocker et al., 1999; Gu et al., 2005; Pedarzani et al., 2005; Otto, 2006; Chen et al., 2014). We have previously examined the contribution of small-conductance calcium-activated potassium (SK) current, M-type potassium current, and A-type potassium current with respect to the asymmetric firing in response to symmetric current ramps (Upchurch et al., 2022). We found that, in the relatively low range of firing frequencies evoked by this type of stimulation, the adaptation induced by these currents does not play a role in shifting action potentials to earlier times during the ramp. However, cholinergic activation has also been shown to activate a non-specific inward cationic current, I_{CAN}, that is thought to be carried by certain TRP channels (Guinamard et al., 2010; Reboreda et al., 2011). Flufenamic acid (FFA) has been shown to block a variety of TRP channels in hippocampal neurons (Partridge and Valenzuela, 2000) and elsewhere (Guinamard et al., 2013). After observing the typical response to CCh, responses to symmetric ramps were recorded while FFA (100 μM) was applied along with CCh (Figure 3A and 3B). FFA shifted most action potentials back to the up-ramp as shown in the examples in Figure 3A1-3A3 and 3B1-3B3, effectively reversing the shift triggered by CCh. The differences in adaptation index across the three conditions were found to be significantly different by repeated measures ANOVA in both somatic recordings (control 0.35 ± 0.05, CCh -0.36 ± 0.09, CCh+FFA 0.25 ± 0.06; $F(2,16) = 65.835$; $p < 0.0005$; $n = 9$; Figure 3A4) and dendritic recordings (control 0.52 ± 0.02, CCh -0.54 ± 0.11, CCh+FFA 0.20 ± 0.08; $F(2,16) = 60.680$; $p < 0.0005$; $n = 9$; Figure 3B4). Bonferroni-adjusted pairwise comparisons indicated that for somatic recordings, the differences were significantly different between control and CCh ($p < 0.0005$), and between CCh and CCh+FFA ($p < 0.0005$), but not between control and CCh+FFA ($p = 0.43$). For dendritic recordings, the differences were significantly different between control and CCh ($p < 0.0005$), CCh and CCh+FFA ($p < 0.0005$), and control and CCh+FFA ($p = 0.02$). In most cases, the adaptation index reverted to a positive value with the application of FFA from a negative value in CCh alone, and in all cases was closer to the control value with FFA than with CCh alone. The failure of the adaptation index to return to control values in FFA may reflect an incomplete block of TRP channels or an additional effect of CCh. Overall, these data suggest that the shift later along the ramp associated with cholinergic activity is due, in large part, to activation of TRP channels.

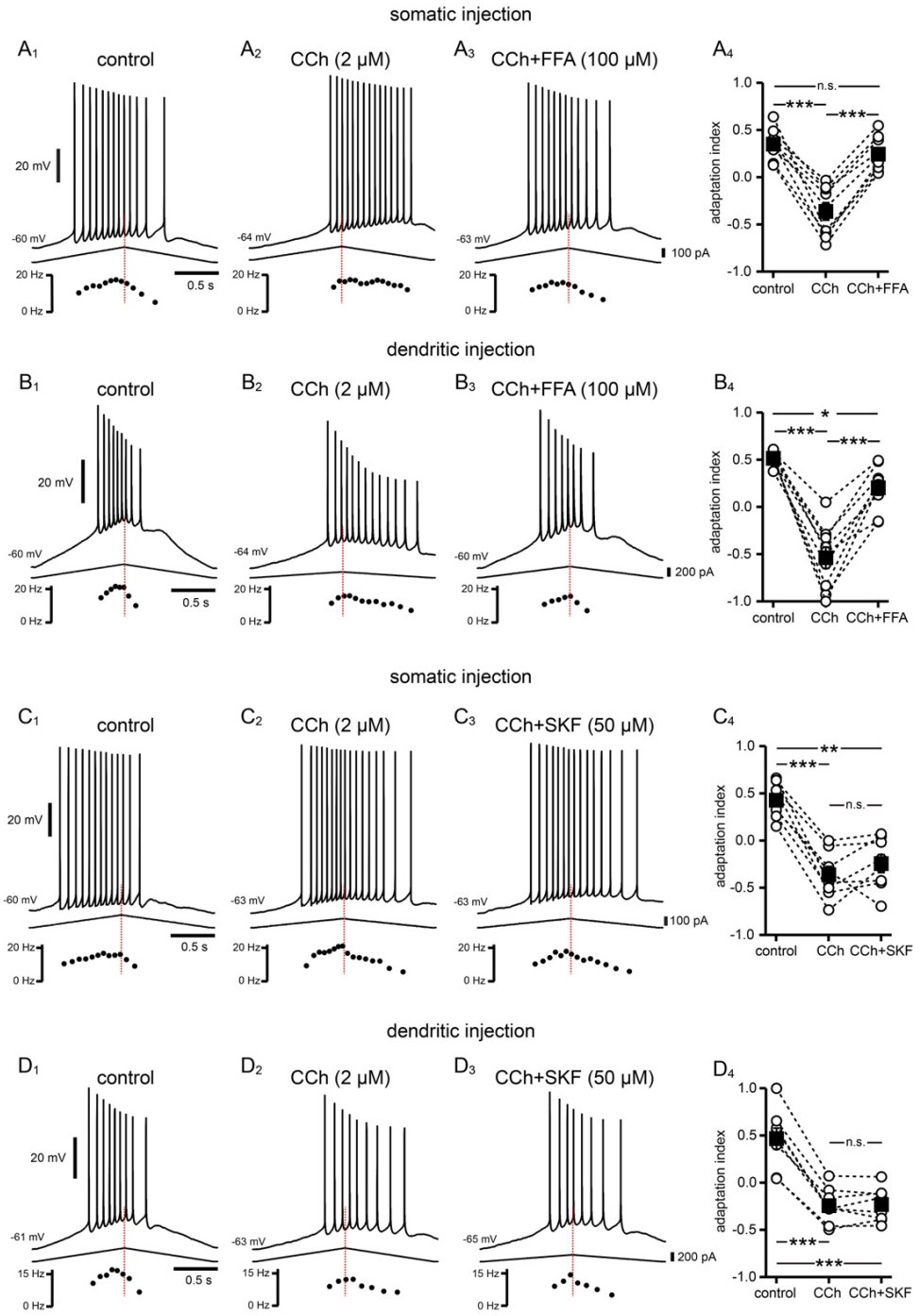

Figure 3. Cholinergic-associated shift in the timing of firing on ramp is mediated by TRP channels, but notably not TRPC channels. A. Voltage traces recorded in the soma for a two second triangular current ramp injected in the soma in control (A1), CCh (2 μM, A2), and CCh + FFA (100 μM, A3) applied subsequently to the same cell. Current traces and instantaneous frequency plots are just below voltage traces. Red dotted line marks the middle of the ramp. Summary data (A4) of the adaptation index for control, CCh, and CCh + FFA (n = 9). B. Same as in A, but for dendritic injection and recordings. Summary data (B4) of the adaptation index for control, CCh, and CCh + FFA (n = 9). Open circles connected by dashed lines represent indices for individual cells, over all three treatments. Black squares with error bars represent group averages ± SEM. C. Voltage traces recorded in the soma for a two second triangular current ramp injected in the soma in control (C1), CCh (2 μM, C2), and CCh + SKF96365 (50 μM, C3) applied subsequently to the same cell. Current traces and instantaneous frequency plots are just below voltage traces. Red dotted line marks the middle of the ramp. Summary data (C4) of the adaptation index for control, CCh, and CCh + SKF96365 (n = 8). D. Same as in C, but for dendritic injection and recordings. Summary data (D4) of the adaptation index for control, CCh, and CCh + SKF96365 (n = 8). *** $p < 0.0005$, ** $p = 0.001$, * $p = 0.02$, n.s. not significant.

The TRPC subfamily has been implicated as being responsible for I_{CAN} in some neurons and is thought to be activated by elements downstream of muscarinic acetylcholine receptor activation (Putney, 2005), which makes it an attractive candidate, mechanistically, for this cholinergic-mediated shift in action potential firing along the depolarizing ramp. Cholinergic stimulation of $G_{q/11}$-coupled mAChRs results in phospholipase C hydrolysis of membrane constituent phosphatidylinositol 4,5-bisphosphate (PIP_2) into inositol 1,4,5-trisphosphate (IP_3) and diacylglycerol (DAG). IP_3 stimulates IP_3 receptor (IP_3R) associated Ca^{2+} release from the endoplasmic reticulum, regulating TRPC channel activity via calmodulin (Zhu, 2005), while DAG activates TRPC channels directly (Hofmann et al., 1999; Mederos Y Schnitzler et al., 2018).

In a set of experiments similar to those above, the TRPC-specific antagonist SKF96365 (50 μM) was added after CCh was applied (Figure 3C and 3D). The differences in adaptation index across the three conditions were found to be significantly different by repeated measures ANOVA in somatic recordings (control 0.43 ± 0.07, CCh -0.36 ± 0.09, CCh+SKF -0.24 ± 0.1; $F(2,14) = 42.453$; $p < 0.0005$; $n = 8$; Figure 3C4) and dendritic recordings (control 0.47 ± 0.1, CCh -0.24 ± 0.07, CCh+SKF -0.23 ± 0.06; $F(2,14) = 118.541$; $p < 0.0005$; $n = 8$; Figure 3D4). However, Bonferroni-adjusted pairwise comparisons demonstrated that the significant differences lie both between control and CCh (soma $p < 0.0005$; dendrite $p < 0.0005$) and control and CCh+SKF (soma $p = 0.001$; dendrite $p < 0.0005$), not between CCh and CCh+SKF (soma $p = 0.68$; dendrite $p = 1.00$). Thus, SKF96365 did not significantly shift the adaptation index in the same manner as did FFA, suggesting that the TRP channels involved in the CCh-mediated forward shift are not of the TRPC subtype.

TRPM4 has likewise been implicated in depolarization associated with G_q-coupled signaling (Launay et al., 2002; Dutta Banik et al., 2018). TRPM4 is activated by Ca^{2+} binding to the cytoplasmic side combined with depolarization (Nilius et al., 2003; Autzen et al., 2018), but the channels are impermeable to Ca^{2+}. Instead, TRPM4 channels facilitate a rise in $[Ca^{2+}]_i$ indirectly, by depolarizing the membrane potential (Launay et al., 2002) and therefore activating voltage-gated Ca^{2+} channels (Li et al., 2021). Cationic current through these channels and the resulting $[Ca^{2+}]_i$ elevation has been implicated in bursting, persistent firing, and oscillatory activity in some neurons (Lin et al., 2017; O'Malley et al., 2020; Li et al., 2021). In order to investigate the involvement of TRPM4 channels in the cholinergic-mediated shift in adaptation index, the TRPM4 antagonist CBA (50 μM) was added after recording the response to CCh (Figure 4A and 4B). Repeated measures ANOVA showed significant differences in the adaptation indices in somatic recordings (control 0.29 ± 0.05, CCh -0.37 ± 0.10, CCh+CBA 0.17 ± 0.01; $F(2,16) = 66.257$; $p < 0.0005$; $n = 9$; Figure 4A4) and dendritic recordings (control 0.39 ± 0.07, CCh -0.41 ± 0.10, CCh+CBA 0.08 ± 0.05; $F(2,16) = 34.848$; $p < 0.0005$; $n = 9$; Figure 4B4). Bonferroni-corrected pairwise comparisons indicated that for somatic recordings, the differences were significant between control and CCh ($p < 0.0005$), and between CCh and CCh+CBA ($p < 0.0005$), but not between control and CCh+CBA ($p = 0.16$). For dendritic recordings, Bonferroni-corrected pairwise comparisons showed that the differences were significant

between control and CCh ($p < 0.0005$), between CCh and CCh+CBA ($p = 0.002$), and between control and CCh+CBA ($p = 0.02$). In most cells, the adaptation index became negative in CCh and reverted to a positive value with the addition of CBA, and in all cases the adaptation index was higher in CCh+CBA than in CCh alone.

In order to corroborate that the effect of CBA is due to block of TRPM4 channels, we investigated the effect of a second TRPM4 antagonist, 9-phenanthrol, added to CCh in somatic recordings. Figure 4C illustrates the shift of most of the spiking activity towards the up-ramp, moving the adaptation ratio in the positive direction, when 9-phenanthrol (100 μM) was applied on top of CCh. The differences in adaptation index between groups are significant, as demonstrated by repeated measures ANOVA (control 0.40 ± 0.03, CCh -0.14 ± 0.06, CCh+9Ph 0.19 ± 0.06; $F(2,14) = 57.640$; $p < 0.0005$; $n = 8$; Figure 4C4). Bonferroni-corrected pairwise comparisons indicated that the differences were significant between control and CCh ($p < 0.0005$), between CCh and CCh+9Ph ($p = 0.001$), and between control and CCh+9Ph ($p = 0.03$).

Taken together, these data with the non-selective TRP channel blocker FFA, the TRPC channel blocker SKF96365, and two different TRPM4 antagonists suggest that the shift in adaptation index that we see with CCh is at least partially mediated through activation of TRPM4, rather than TRPC, channels.

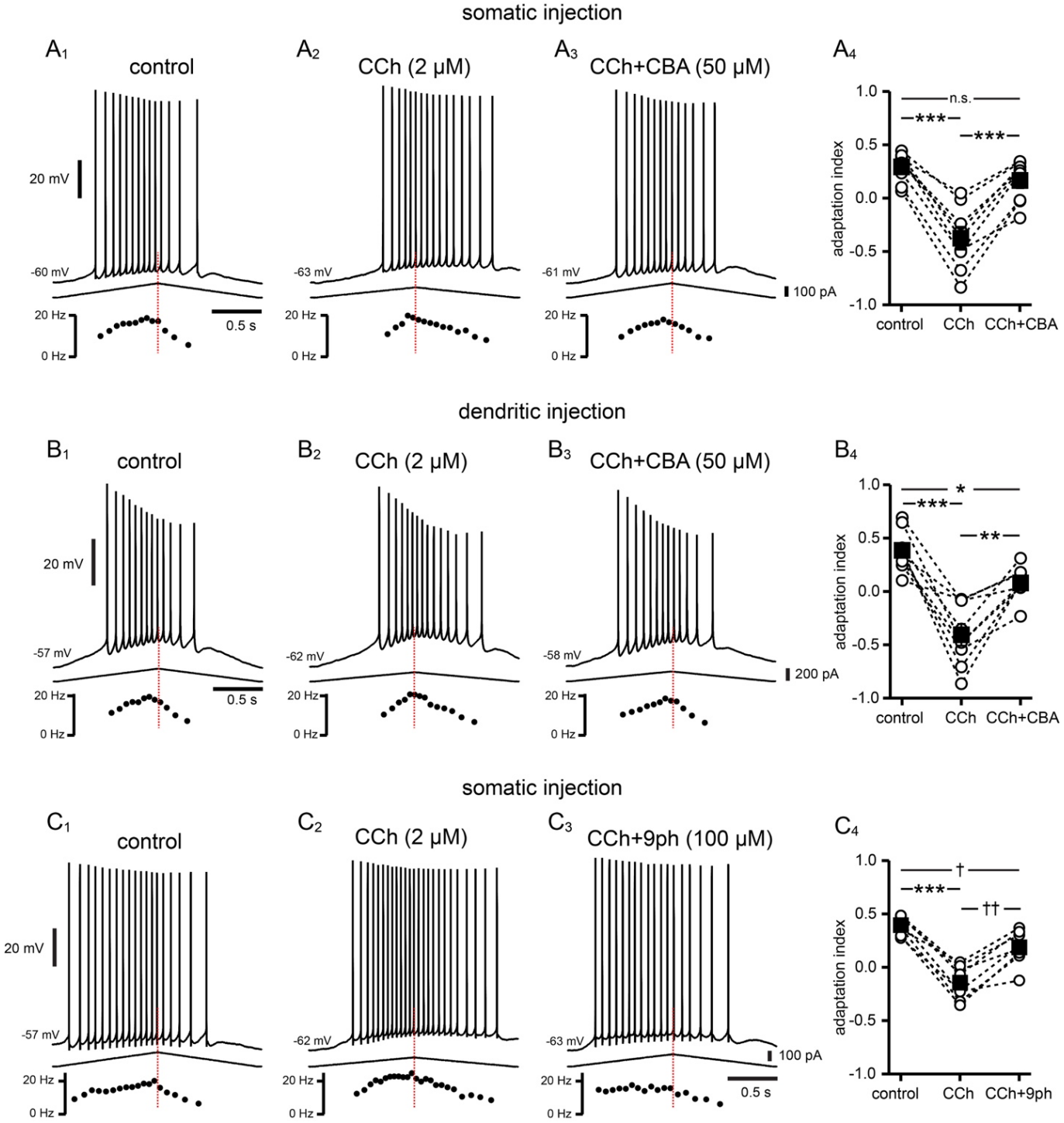

Figure 4. Cholinergic-associated shift in the timing of firing on ramp is mediated by TRPM4 channels.
A. Voltage traces recorded in the soma for a two second triangular current ramp injected in the soma in control (A1), CCh (2 μM, A2), and CCh + CBA (50 μM, A3) applied subsequently to the same cell. Current traces and instantaneous frequency plots are just below voltage traces. Red dotted line marks the middle of the ramp. Summary data (A4) of the adaptation index for control, CCh, and CCh + CBA (n = 9). Open circles connected by dashed lines represent indices for individual cells, over all three treatments. Black squares with error bars represent group averages ± SEM. B. Same as in A, but for dendritic injection and recordings. Summary data (B4) of the adaptation index for control, CCh, and CCh + CBA (n = 9). C. Same as A, but for control (C1), CCh (2 μM, C2), and CCh + 9-phenanthrol (100 μM, C3) applied subsequently to the same cell. Summary data (C4) of the adaptation index for control, CCh, and CCh + 9-phenanthrol (n = 8). *** $p < 0.0005$, ** $p = 0.002$, * $p = 0.02$, †† $p = 0.001$, † $p = 0.03$, n.s. not significant.

Multicompartmental modeling of cholinergic modulation of asymmetric firing responses

We next turned to our detailed multicompartmental model, in order to help identify the underlying mechanisms that contribute to the cholinergic modulation that we observe experimentally *in vitro*. The model was implemented in a reconstructed morphology (Megías et al., 2001) with 144 compartments (Figure 5A), each of which can be represented with an equivalent circuit as shown in Figure 5B. Channel conductance densities and kinetics were heterogeneous as described in the Methods. Figure 5C illustrates the cholinergic second messenger cascade that activates TRPM4. We hypothesize Ca^{2+} entering via voltage-gated Ca^{2+} channels, activated by ramp depolarization, and elevated IP_3, due to PIP_2 cleavage following activation of the M_1 receptor, converge upon the IP_3 receptor and are both required to open the receptor channel and allow release of Ca^{2+} from the endoplasmic reticulum. The calcium handling for the model (Figure 5D) was modified from (Ashhad and Narayanan, 2013) as described in the Methods. Essentially, the model performs a material balance on the Ca^{2+} ions to provide estimated free Ca^{2+} concentrations in concentric shells beneath the membrane and in a hypothesized nanodomain. We hypothesize that the Ca^{2+} binding site on the TRPM4 channel and the site of Ca^{2+} release from the IP_3 receptor are co-localized, creating a nanodomain with spatially restricted high concentrations of Ca^{2+} sensed by the TRPM4 channel. In HEK-293 cells overexpressing TRPM4 channels, extracellular application of ATP, a ligand for G_q-linked receptors, induced a large, global increase in $[Ca^{2+}]_i$, followed by secondary $[Ca^{2+}]_i$ transients released through IP_3 receptors. It was the smaller, secondary $[Ca^{2+}]_i$ transients that were temporally linked to inward current via TRPM4 channels (Launay et al., 2002), suggesting a co-localization of IP_3R and TRPM4 channels. Subsequent studies in smooth muscle cells, in which TRPM4 is highly expressed and plays a major role in vasoconstriction, have demonstrated that the calcium source associated with TRPM4 activation is likely to be IP_3R-mediated calcium release from the sarcoplasmic reticulum (Gonzales et al., 2010; Gonzales and Earley, 2012). These studies are consistent with our assumption of a nanodomain comprising IP_3R and TRPM4 channels. IP_3 concentration was set to one value for control and to a higher value to simulate the presence of CCh.

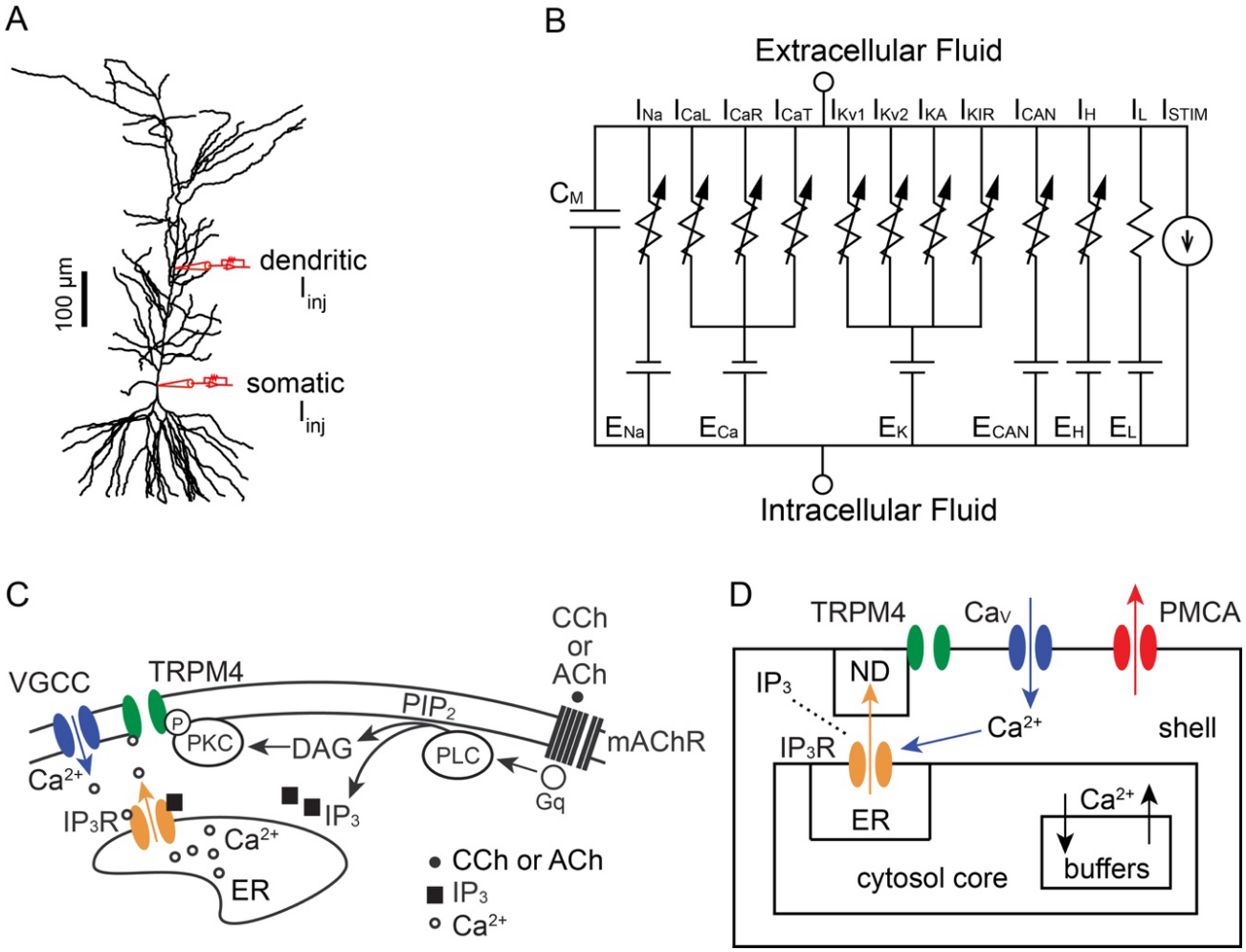

Figure 5. Model Schematics.
A. Reconstructed morphology ported to NEURON simulation program, with somatic and dendritic current injection sites labeled. B. Equivalent circuit diagram, with the reversal potentials for each channel indicated by E_X. The following currents were modeled using Ohmic drive and conductances in parallel with a membrane capacitance (C_M): a Na^+ current (I_{Na}), L-type (I_{CaL}), R-type (I_{CaR}), and T-type (I_{CaT}) Ca^{2+} currents, two delayed rectifiers (I_{Kv1} and I_{Kv2}), an A-type K^+ current (I_A), an inward rectifying potassium current (I_{KIR}), a nonspecific Ca^{2+}-activated current (I_{CAN}), a hyperpolarization-activated mixed cationic h-current (I_h), and a leak current (I_L). C. mAChR signaling cascade. D. Simplified model calcium handling schematic. For simplicity, only one annulus (shell) is shown and the rest are represented as the core. Ca^{2+} enters via voltage-gated Ca^{2+} channels (Ca_V) and is removed by the plasma membrane Ca^{2+} pump. Inside the cell, buffering and the endoplasmic reticulum (ER) are also modeled. The TRPM4 channel is not permeable to Ca^{2+} and senses Ca^{2+} concentration in a nanodomain (ND) due to its assumed close proximity to the IP_3 receptor (IP_3R). VGCC voltage-gated calcium channel; IP_3 inositol 1,4,5-trisphosphate; IP_3R IP_3 receptor; PKC phosphokinase C; DAG diacylglycerol; PLC phospholipase C; ER endoplasmic reticulum; PIP_2 phosphatidylinositol 4,5-bisphosphate; ND nanodomain; PMCA plasma membrane Ca^{2+} ATPase.

Figure 6 shows the simulated results for short triangular ramps of injected current. The control simulation (low value of IP_3 concentration) for a short somatic ramp in Figure 6A1 captures the experimentally observed decrease in spike number and frequency on the down-ramp as compared to the up-ramp (adaptation index = 0.38), as well as a slight decrease in spike amplitude. Increasing IP_3 concentration to a higher value to simulate the bath application of CCh (Figure 6B1) replicates the experimentally observed shift in adaptation index, with more spikes occurring on the down-ramp as compared to the up-ramp (adaptation index = -0.50). The dendritic ramps in Figure 6C1 and 6D1 also replicate the experimentally observed rightward shift in spike timing with CCh simulation (adaptation indices: low IP_3 = 0.45; high IP_3 = -0.43), with the additional observation that the decrease in spike amplitude is greater for dendritic ramps, consistent with our previous modeling that incorporates more slow inactivation of the Na_V channel in the dendrites as compared to the soma (Upchurch et al., 2022). Plots of instantaneous frequency versus current injection shown in Figure 6A2, 6B2, 6C2 and 6D2 capture the experimentally observed higher frequencies on the up-ramp in control, and higher frequencies on the down-ramp when IP_3 concentration is high.

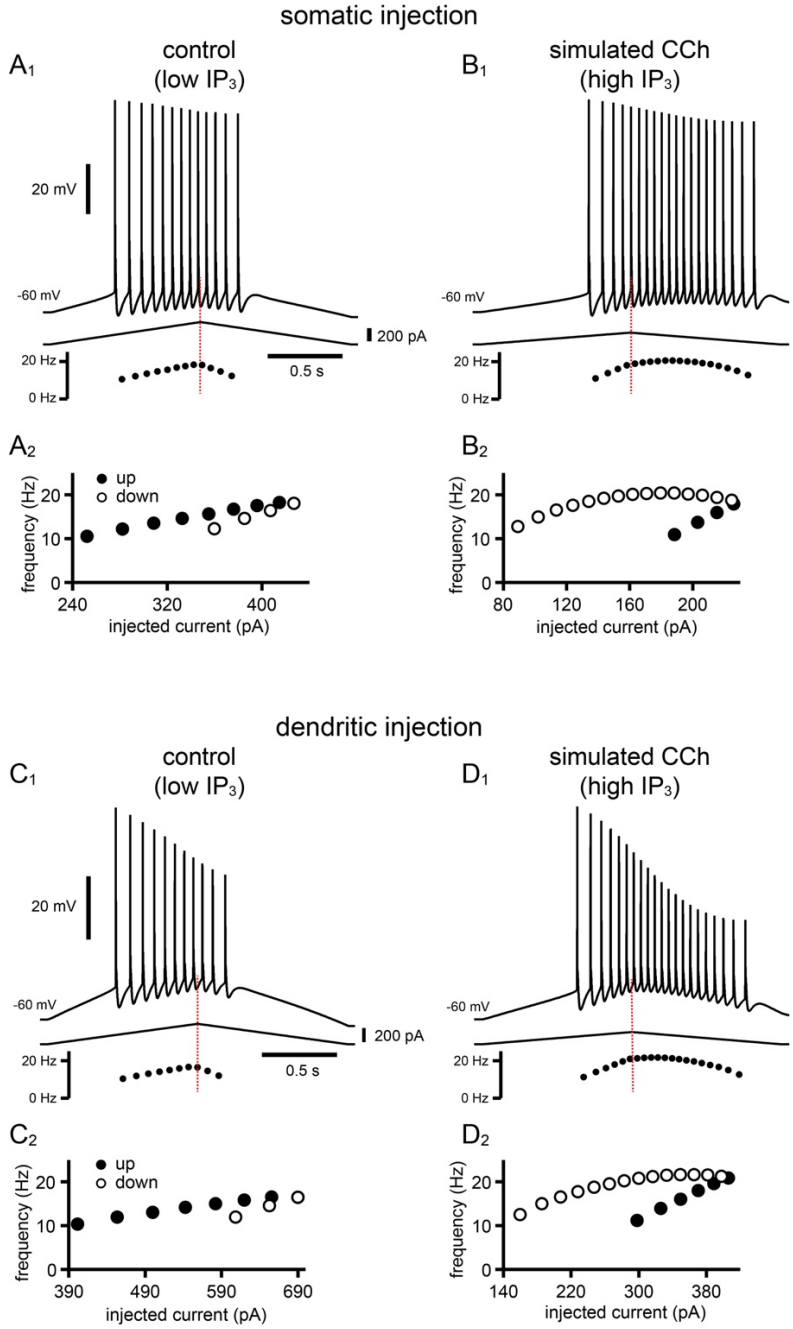

Figure 6. Simulated short ramps for both soma and dendrites in simulated control (low IP_3) and simulated CCh (high IP_3).

A. Simulated somatic control. A1. Simulated voltage traces (top) during a two second triangular current ramp (just below voltage trace) with the reciprocal of the interspike interval (ISI) plotted as the instantaneous frequency at the ISI midpoint (below current ramp). Vertical dashed red line shows the peak of the current ramp. A2. The instantaneous frequency plotted as a function of injected current at the midpoint. The slower frequencies and fewer ISIs on the down-ramp (open circles) versus the up-ramp (closed circles) show hysteresis due to adaptation mediated by long-term inactivation of the sodium channel. B. Same format as A but for simulated application of CCh. B1. Note the firing pattern is shifted to the right compared to A1. B2. The hysteresis is in the opposite direction because the activation of TRPM4 by Ca^{2+} accumulation obscures and overwhelms adaptation. C. Same as A but for simulated dendritic control. D. Same as B but for simulated effect of CCh as recorded in the dendrites.

Evidence for tight coupling between TRPM4 and the calcium source that activates it

Figure 7A1 and 7B1 repeat panel A1 and B1 from the previous figure, while Figure 7C1 is the result of increasing IP_3 concentration after removing the Ca^{2+} nanodomain from the model. Figure 7A2, 7B2, and 7C2 show the nanomolar [Ca^{2+}] increases in the outer shell, both in the simulated control and CCh conditions. Note that in control (A2) and with high IP_3 but no nanodomain (C2), the Ca^{2+} concentration in the outer shell begins to decrease prior to cessation of spiking (see red arrows), due to the decrease in frequency during the down-ramp because of the Na^+ channel long-term inactivation (Upchurch et al., 2022). Figure 7A3 shows no noticeable micromolar increase in Ca^{2+} concentration in the nanodomain under control conditions. On the other hand, in the simulated presence of CCh, the elevated IP_3 concentrations allow activation of the IP_3 receptor to flood the nanodomain with micromolar Ca^{2+} (Figure 7B3), which activates TRPM4 channels (Figure 7B4). The TRPM4 current is responsible for the increased spiking on the down-ramp. This mechanism sets up a positive feedback between Ca^{2+} entry and the inward TRPM4 current, which increases the firing frequency by shortening the interspike intervals. This process overcomes both the decrease in injected current and the long-term inactivation of the Na^+ current. In this situation, the neuron will stop firing only when the sum of the inward currents fails to reach threshold, which occurs near the end of the down-ramp; the vertical black dashed line in 7B marks the termination of the down-ramp. Without a nanodomain (Figure 7C3), elevation of IP_3 concentration combined with the nanomolar increases in Ca^{2+} in the outer shell is insufficient in our model to activate TRPM4 (Figure 7C4). If the half-activation of TRPM4 is reduced to nanomolar concentrations, 100 pA or more of baseline TRPM4 current is elicited, contrary to experiments in which application of FFA or CBA in the presence of CCh elicited no noticeable change in membrane potential (not shown).

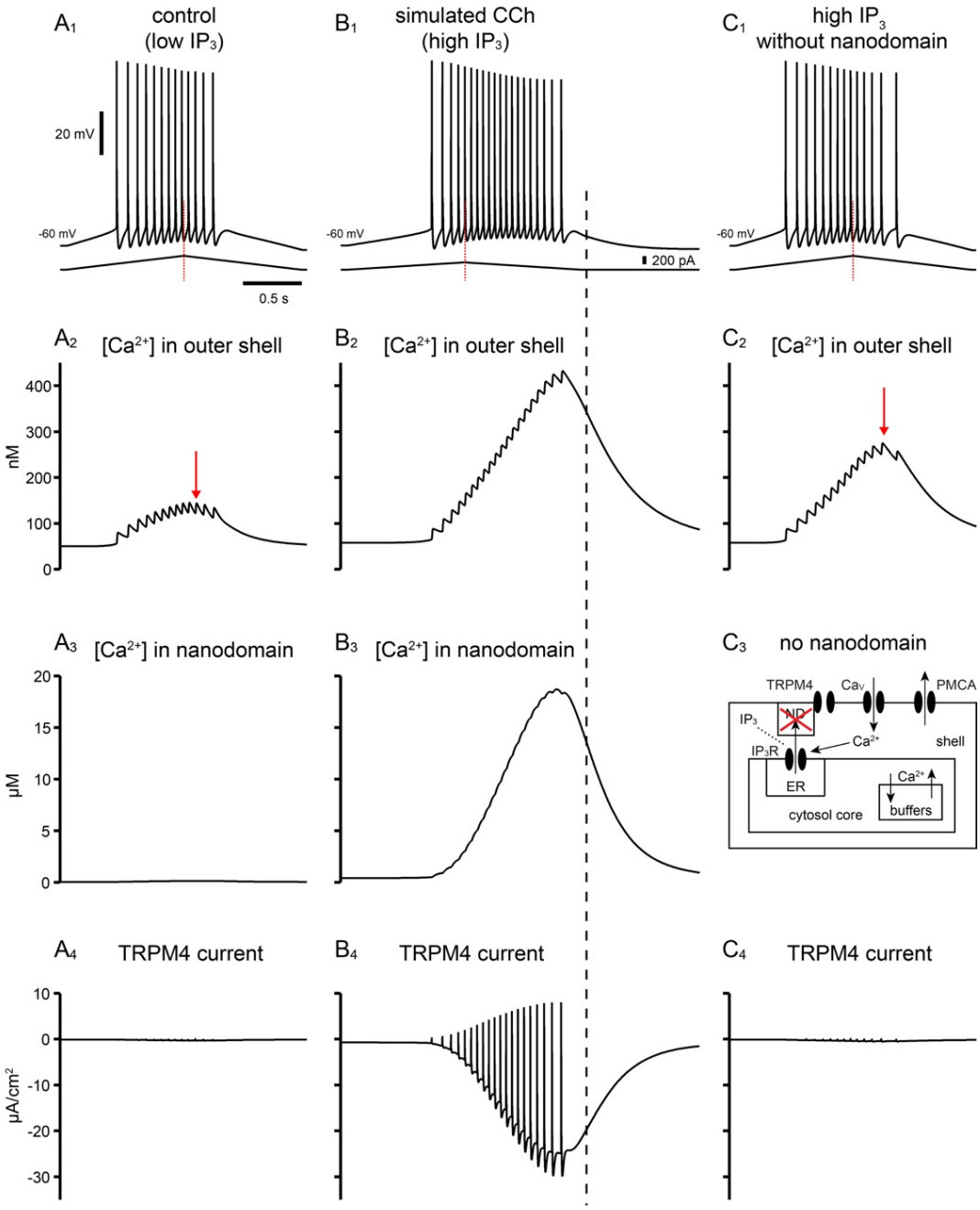

Figure 7. In the model, TRPM4 requires a nanodomain of high calcium to capture response seen with cholinergic activation in experiments.

A. Simulated somatic recordings in control (low IP_3). A1. Repeated voltage traces and current ramp from Figure 6A1. A2. Nanomolar Ca^{2+} concentration in outer shell beneath the cell membrane. A3. The nanodomain Ca^{2+} concentration is not elevated with low levels of IP_3 that simulate control. A4. There is negligible TRPM4 activation. B. Simulated somatic recordings in CCh (high IP_3). B1. Repeated voltage traces and current ramp from Figure 6B1. B2. Nanomolar Ca^{2+} concentration in outer shell beneath the cell membrane is elevated due to increased spiking on the down-ramp. B3. The nanodomain Ca^{2+} concentration reached micromolar concentrations with high levels of IP_3 that simulate application of CCh. B4. TRPM4 is robustly activated. Black dashed line marks the end of the injected current ramp, highlighting that the return to baseline of Ca^{2+} and TRPM4 current lags behind injected current ramp. C. Simulated somatic recordings in CCh (high IP_3) with no nanodomain. C1. Voltage traces and current ramp. Note that more ramp current is required to achieve the same firing rates as were achieved in B1. C2. Nanomolar Ca^{2+} concentration in outer shell beneath the cell membrane. C3. No nanodomain. C4. There is negligible TRPM4 activation. In A2 and C2, the red arrows point to when the $[Ca^{2+}]$ in the outer shell starts decreasing while the neuron keeps firing, as opposed to B2.

In order to test experimentally the model prediction that the highly localized Ca^{2+} elevation in a nanodomain between the ER and TRPM4 channels gives rise to the CCh-mediated shift in spiking, the calcium chelator BAPTA was included in the recording pipette, and somatic recordings obtained before and after addition of CCh. In Figure 8, control data reflect the effect of BAPTA before the addition of CCh, rather than control data such as in previous figures, because the dialysis occurred quickly. In all cases, the addition of BAPTA to the intracellular solution tends to shift the firing earlier in the ramp, with few spikes on the down-ramp, therefore making the adaptation index closer to 1. In Figure 8A, 10 mM BAPTA was included in the internal solution. Upon addition of CCh in the bath, the adaptation index became significantly smaller, despite the presence of BAPTA, as per a paired t-test (control 0.82 ± 0.05, CCh -0.12 ± 0.11; $t(9) = 8.594$; $p < 0.0005$; $n = 10$), suggesting that 10 mM BAPTA did not occlude the CCh-mediated shift. It has been shown that a higher concentration of BAPTA may be required to prevent TRPM4 channel activation (Pace et al., 2007; Picardo et al., 2019), therefore, in Figure 8B, BAPTA in the internal solution was increased to 30 mM. With a free $[Ca^{2+}]_i$ of 100 nM (see Methods), CCh never produced negative adaptation indices that were seen in previous figures. CCh still had a significant effect on the adaptation index, as per a paired t-test (control 0.62 ± 0.05, CCh 0.37 ± 0.06; $t(7) = 5.069$; $p = 0.001$; $n = 8$). However, when the free $[Ca^{2+}]_i$ was 10 nM (Figure 8C), the adaptation index did not change significantly when CCh was applied in the bath (control 0.73 ± 0.03, CCh 0.76 ± 0.03; $t(11) = 0.776$; $p = 0.45$; $n = 12$). These data demonstrate that a concentration of BAPTA higher than the one that is normally used to disrupt Ca^{2+}-dependent mechanisms (Harney et al., 2006) is required to prevent TRPM4 channel activation, and that the free $[Ca^{2+}]_I$ of <100 nM is necessary to disrupt TRPM4 activation. Together, these data suggest a close physical relationship between the source of Ca^{2+} and TRPM4 channels.

SK can be activated by IP_3R-mediated Ca^{2+} elevation (Power and Sah, 2008). In a previous study, we found that BAPTA at 5 mM can mimic SK block (Combe et al., 2018), presumably by interfering with calcium activation. That the experiments in Figure 8 required 30 mM BAPTA and free $[Ca^{2+}]_i$ buffered to 10 nM in order to prevent TRPM4 activation suggests that TRPM4 is more tightly coupled to IP_3R-Ca^{2+} than SK channels are. In arterial smooth muscle cells, TRPM4 channels are thought to be within 50 nm of IP_3R (Gonzales and Earley, 2012). While we do not know if this is generalizable to TRPM4 and IP_3R in neurons, our model predicts TRPM4 activation by a calcium nanodomain, which is supported by our experimental results.

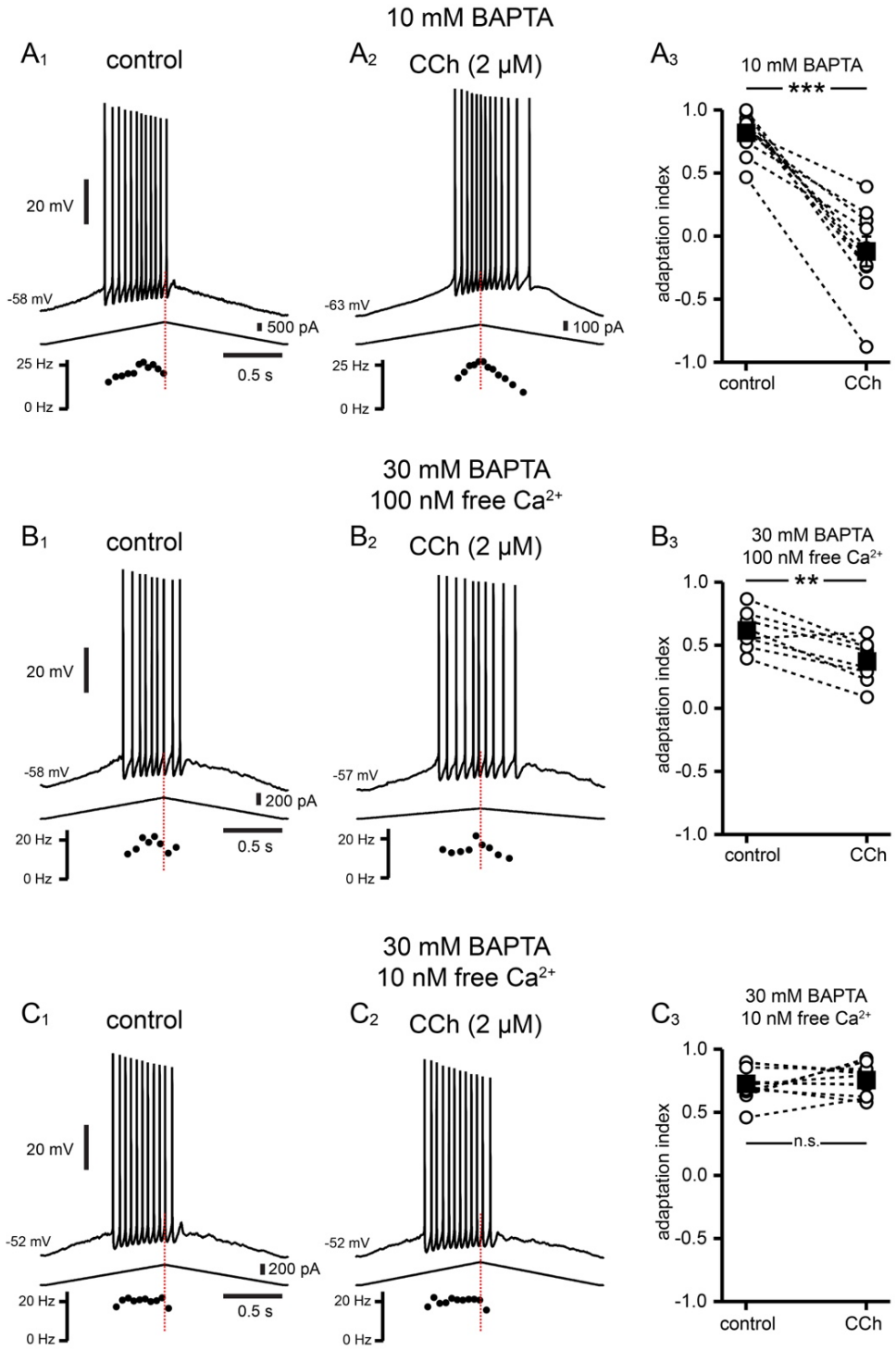

Figure 8. A high concentration of BAPTA is required to interfere with CCh-mediated shift in firing along ramp.
A. Voltage traces recorded in the soma during intracellular dialysis with 10 mM BAPTA, for a two second triangular current ramp injected in the soma before (A1), and after superfusion with CCh (2 μM, A2). Current traces and instantaneous frequency plots are just below voltage traces. Red dotted line marks the middle of the ramp. Summary data (A3) of the adaptation index for control and CCh (n = 10). Open circles connected by dashed lines represent ratios for individual cells, before and after CCh. Black squares with error bars represent group averages ± SEM. B. Same as A, but intracellular dialysis is with 30 mM BAPTA and 100 nM free [Ca^{2+}]. Summary data (B3) of the adaptation index for control and CCh (n = 8). C. Same as A, but intracellular dialysis is with 30 mM BAPTA and 10 nM free [Ca^{2+}]. Summary data (C3) of the adaptation index for control and CCh (n = 12). *** $p < 0.0005$, ** $p = 0.001$, n.s. not significant.

Discussion

Summary of major results

Whereas place cell firing can only be observed *in vivo*, our bidirectional approach of modeling place cell firing *in vitro* and *in silico* can be precisely targeted to uncover molecular mechanisms responsible for modulation of firing patterns that lead to place cell firing *in vivo*. Manipulations that are difficult or impossible even the *in vitro* preparation can be carried out *in silico* using our detailed multicompartmental model, with the added benefit that the model is transparent. All underlying state variables (ion concentrations, channel open fractions) are accessible so that mechanisms can be positively identified, facilitating design of experiments to test the putative mechanisms.

In this study we show that: 1) cholinergic receptor activation shifts the adapting firing pattern from earlier to later during a depolarizing ramp, through 2) activation of I_{CAN} mediated by TRP channels, most likely of the TRPM4 subtype; 3) multicompartmental modeling suggests a close physical relationship between the source of Ca^{2+} increase and the TRPM4 channels; 4) the model prediction is supported by recordings showing that a very high concentration of BAPTA (30 mM), combined with buffering $[Ca^{2+}]_i$ at 10 nM are required to prevent the cholinergic-mediated rightward shift. Cholinergic stimulation elevates IP_3, which increases the sensitivity of IP_3R to Ca^{2+}. Thus, IP_3R functions as a coincidence detector (Berridge, 1998) to detect simultaneous elevation of IP_3 and Ca^{2+}. Together, these results suggest that, at the cell level, IP_3R is the locus that requires both cholinergic activation and activation of voltage-gated Ca^{2+} channels during sustained depolarization to produce the rightward shift in firing rate along the ramp. More broadly, our results suggest that some rapid changes to place cell firing could be triggered via neuromodulation of intrinsic excitability, distinct from longer lasting experience-dependent changes that are brought about by synaptic and structural plasticity. Specifically, we show that increasing levels of ACh could lead to forward shifts in place cell firing, whereas decreasing levels of ACh could contribute to backwards shifts.

Mystery current identified

Muscarinic activation of Ca^{2+}-dependent nonselective cation current in rat CA1 pyramidal neurons, with possible involvement of IP_3, has been known for nearly three decades (Colino and Halliwell, 1993; Fraser and MacVicar, 1996). A previous study (Yamada-Hanff and Bean, 2013) found that in mouse CA1 neurons as well, muscarinic stimulation not only inhibits background potassium currents but also activates a nonselective cation current. They found that the latter effect was dominant and in fact converted CA1 pyramidal neurons into pacemakers with the application of 5-25 μM acetylcholine, 5-25 μM carbachol, or 5-10 μM oxotremorine-M. They suggested TRPC channels might mediate this current but were unable to positively identify the source of the nonselective cation current.

Our most surprising finding was that TRPC channels did not seem to play a role in cholinergic modulation of the firing pattern along a triangular ramp. TRPC channels have been implicated in cholinergic signaling via direct activation by DAG, one of the two bioactive molecules generated by PLC hydrolysis of PIP_2 (the other being IP_3). Cholinergic-associated persistent firing, whereby neurons continue to fire after a depolarizing stimulus has ceased, has been attributed to activation of TRPC channels (Zhang et al., 2011; Arboit et al., 2020). However, the presence of cholinergic-induced persistent firing in TRPC knockout mice has called this into question (Egorov et al., 2019). Based on our results, TRPM4 primarily mediates the Ca^{2+}-activated nonselective cation current evoked by cholinergic modulation in our experimental conditions. Similarly, recently persistent firing in thalamic neurons generated upon Ca^{2+} influx via T-type channels was found to involve TRPM4 (O'Malley et al., 2020); delayed bursting in a subtype of cerebellar granular cells was also shown to be mediated by TRPM4 channels (Masoli et al., 2020).

Nanodomain resulting from putative colocalization of IP_3R and TRPM4

Our modeling results imply that TRPM4 has privileged access to the Ca^{2+} released by IP_3 receptors from the endoplasmic reticulum. Nanodomains achieve micromolar concentrations of Ca^{2+}, whereas microdomains (like the multicompartmental model's outer shell) achieve submicromolar concentrations (Fakler and Adelman, 2008). The affinity of TRPM4 for Ca^{2+} is heavily dependent on the availability of PIP_2 (Nilius et al., 2006) and binding of ATP and calmodulin or PKC-dependent phosphorylation (Nilius et al., 2005), which all function to increase the sensitivity of TRPM4 channels for Ca^{2+}. If under our conditions, the dependence of TRPM4 channels on $[Ca^{2+}]$ has a much lower EC_{50} and/or is much steeper than in the model we implemented (Nilius et al., 2004), perhaps the nanomolar Ca^{2+} in the outer shell could be sufficient to activate TRPM4. However, the experimental result that 30 mM BAPTA was required to block the TRPM4 channel's access to the Ca^{2+} released by the IP_3R argues for a spatially restricted nanodomain. Such close apposition of IP_3Rs and TRPM4 channels has been directly observed in smooth muscle cells (Provence et al., 2017). We suggest that the cholinergic shift is only occluded when free $[Ca^{2+}]_i$ is buffered at 10 nM but not 100 nM with 30 mM BAPTA in the pipette because 10 nM is not sufficient to activate IP_3R but 100 nM is (Bezprozvanny et al., 1991).

Convergence of pharmacological blockers

One caveat for our experimental results is that TRP channel blockers, like most drugs, have been reported to have some non-specific effects. In cardiac cells, both CBA and 9-phenanthrol have been shown to decrease the Ito1 potassium current, attributed to Kv4.3 (Veress et al., 2018; Dienes et al., 2021) and a late sodium current (Hou et al., 2018; Dienes et al., 2021). Kv4.3 is likely more important in interneurons than in pyramidal cells in the CA1 area (Martina et al., 1998), and neither of the two currents are affected

by FFA at the concentration we used here (Guinamard et al., 2013). The other reported non-specific effects do not overlap between the three blockers, flufenamic acid, CBA and 9-phenanthrol (Simard et al., 2012; Guinamard et al., 2013; Veress et al., 2018; Dienes et al., 2021). The convergent effects of these three distinct drugs implicate TRPM4 channels as the most probable effector of the CCh-mediated modulation of rate hastening.

Diverse cholinergic effects on CA1 pyramidal neurons

In CA1 pyramidal neurons, ACh binding to muscarinic receptors results in neuromodulation of neuronal excitability and presynaptic release probability. In our study, focused on intrinsic properties, the predominant effect of ACh and CCh was to activate TRPM4 channels; however, the effect of ACh on CA1 pyramidal cells *in vivo* is multipronged. Muscarinic effects on the M-type and SK K^+ currents in Ca1 pyramidal neurons are described in earlier sections. The effects of ACh on I_{CAN} and SK are mediated by M_1 (G_q) receptors (Dasari and Gulledge, 2011). Synaptic depression of Schaffer collateral inputs to CA1 is mediated by M_4 (G_i) receptors (Dasari and Gulledge, 2011) located on presynaptic glutamatergic terminals, and synaptic depression of temporoammonic pathway glutamatergic inputs to CA1 is mediated by M_3 (G_q) receptors (Palacios-Filardo et al., 2021). Therefore, the down-regulation of these afferents justifies the use of smaller depolarizing current ramps in our recordings in the presence of carbachol, because less current injection is required to produce the same output frequencies due to enhanced intrinsic excitability in carbachol.

Previously, ACh was thought to act in a manner consistent with volume transmission (Dannenberg et al., 2017). Recently, this view has been challenged by the finding that all hippocampal cholinergic terminals form synapses (Takács et al., 2018), and vesicles dock only at synapses. Moreover, they found that the terminals co-released GABA in separate vesicles, and ACh acting on M_2 (G_i) autoreceptors on cholinergic terminals inhibited the release of both ACh and GABA. Future work is required to disentangle the distinct effects of ACh acting at the various muscarinic receptors (M_1-M_5).

ACh, Novelty and Place Field Shifts

Acetylcholine acting at muscarinic receptors has been hypothesized to be a global novelty signal in the dentate gyrus (Gómez-Ocádiz et al., 2022), dorsal hippocampus (Huff et al., 2022), and the parahippocampal gyrus (Frank and Kafkas, 2021). A novel unconditioned stimulus caused a large increase in ACh extracellular levels in the hippocampus, but little locomotion (Acquas et al., 1996). On the other hand, hippocampal ACh release in an animal placed in a novel environment has two components, one related to novelty, that disappears in a familiar environment (Thiel et al., 1998), and one related to motor

activity, associated with increased exploration (Giovannini et al., 2001). Indeed, a recent fiber photometric study showed that part of the population activity in medial septal cholinergic neurons is correlated with the logarithm of running speed (Kopsick et al., 2022). We are primarily interested in the component of the ACh signal related to novelty because of previous studies demonstrating modulation of place cell firing that was more pronounced during the first day in a novel environment (Roth et al., 2012).

In vivo recordings in rats demonstrated that place fields expand and the center of mass shifts backward with respect to the direction of travel on continuous tracks over several laps during each recording session (Mehta et al., 1997, 2000). This phenomenon was predicted by modeling studies that implemented Hebbian plasticity in the form of NMDA-mediated LTP (Abbott and Blum, 1996; Blum and Abbott, 1996), whereby spatially tuned input gradually strengthens over repeated traversals of a place field, causing a CA1 place cell to fire earlier in the place field. NMDA blockers were subsequently shown to occlude the backwards shift of the place field (Ekstrom et al., 2001) and an NMDA agonist partially restored it in aged rats (Burke et al., 2008). Calcium imaging in mice running on a treadmill in a virtual environment showed an abrupt backward shift in place cell firing (relative to where the first episode of place field firing occurred) during the first exposure to a novel environment (Priestley et al., 2022), as well as much smaller backward shifts in place fields in novel environments that leveled off as the animals became more familiar with the environment during subsequent exposures (Dong et al., 2021). These backwards shifts, which were much larger than those observed previously and attributed to Hebbian plasticity, were ascribed to behavioral time scale plasticity, which is also dependent on NMDA receptor activation, and strengthens glutamatergic inputs active during an asymmetric seconds-long window skewed towards synapses activated before a burst triggered by a dendritic plateau (Bittner et al., 2017).

Despite the ability of elegant theories of synaptic plasticity to account for backward shifts in the center of mass of the place field, forward shifts have also been observed. Forward shifting of the center of mass of place field firing occurred, shifting toward prospective goal locations in the continuous T-maze alternation task as a reward was approached (Lee et al., 2006). Thus, task specific demands may allow for the modulation of firing fields by neuromodulators such as ACh and dopamine. In a study that did not involve reward, but only exploration of a novel virtual linear maze (Dong et al., 2021), the center of mass of CA1 place fields in laps 2-4 were forward shifted compared to the first lap, for cells that already had a place field on the first lap. A lap required approximately 25 seconds. Laps 5 and beyond were backward shifted compared to the immediately preceding lap, so averaging over all runs, the place field was shifted backwards. Perhaps, the neuromodulatory environment, including ACh, was different during the first four laps. The data in that study indicated that backward shifting in CA1 in a novel environment is due to a combination of place field expansion, skewness and translation of the point at which peak firing occurs. They suggested that since skewness and width dynamics are inconsistent across studies, multiple mechanisms may be involved in place field shifting.

Our results suggest that increasing levels of ACh could lead to forward shifts in place field center of mass whereas decreasing levels of ACh could contribute to backwards shifts. Since cholinergic activity in CA1 is elevated when animals encounter novel environments, our results with CCh could correspond to an initial encounter with a novel environment, where firing of an existing place cell is shifted “forward” or later during the depolarizing ramp that simulates spatially-tuned input. Our control conditions, then, would be analogous to lower cholinergic tone, occurring as an animal becomes familiar with an environment, and the associated “backward” shift earlier in the depolarizing ramp. The rapid modulation of ion channels by removal of cholinergic tone could therefore provide a possible mechanism for the rapid shifting of place cell firing in a novel versus familiar environment, perhaps complementary to Hebbian plasticity that develops over time.

Implications for place fields in intact rodents

Optogenetic silencing of medial septum cholinergic afferents to CA1 during runs through a place field in a novel environment should partially occlude backwards shifts in place field center on subsequent runs that are due to diminished ACh in a familiar environment. Optogenetic stimulation of the same afferents during runs in a familiar environment should induce forward shifts in place field centers. Behaviorally, it could be informative to design experiments to test the effects of these manipulations on the animal’s subjective sense of position, for example, demonstrated by overshoot or undershoot locations where the animal has been trained to pause.

There is a growing realization that there may be multiple mechanisms for place field shifting in addition to the well-known mechanisms for backwards shifts dependent on Hebbian plasticity (Blum and Abbott, 1996; Mehta et al., 2000; Ekstrom et al., 2001; Burke et al., 2008; Roth et al., 2012) or, more recently, behavioral timescale synaptic plasticity (Priestley et al., 2022). We propose that neuromodulation of intrinsic properties by ACh, and potentially other neuromodulators like dopamine, provide an additional level of modulatory control in parallel with synaptic plasticity mechanisms, contributing to rapid place field shifts.

Materials and Methods

Experimental methods

Slice preparation. All the procedures described below were conducted according to protocols developed by following guidelines on the responsible use of laboratory animals in research from the National Institutes of Health and approved by the Louisiana State University Health Sciences Center-New Orleans Institutional Animal Care and Use Committee. Animals were housed in pairs, whenever possible; in the

event of single housing, Bed-r'nest pucks (Andersons Lab Bedding) were provided for enrichment purposes.

For these experiments, 400 µm-thick slices were prepared from 7 to 11-week-old male Sprague Dawley rats as previously described (Combe et al., 2018). Briefly, rats were deeply anesthetized via intraperitoneal injection of ketamine and xylazine (90 and 10 mg/kg, respectively), until the disappearance of the toe-pinch and palpebral reflexes. After trans-cardiac perfusion with ice-cold solution, decapitation, and rapid removal of the brains, transverse hippocampal slices were cut using a vibratome. Slices were then transferred to a chamber filled with an oxygenated artificial cerebro-spinal fluid (ACSF) containing, in mM: NaCl 125, $NaHCO_3$ 25, KCl 2.5, NaH_2PO_4 1.25, $MgCl_2$ 1, $CaCl_2$ 2, dextrose 25, ascorbate 1, sodium pyruvate 3.

Patch clamp electrophysiology. After recovery, individual slices were transferred to a submerged recording chamber, and superfused with ACSF at about 2 ml/min; the solution was warmed through an inline heater and measured to keep it at a temperature of 34-36°C in the chamber.

CA1 pyramidal cells were identified via differential interference contrast-infrared video microscopy. Whole-cell current clamp recordings were made using Dagan BVC 700A amplifiers in the active "bridge" mode. Recording pipettes were filled with an internal solution that contained, in mM: potassium methanesulphonate 125, KCl 20, HEPES 10, EGTA 0.5, NaCl 4, Mg_2ATP 4, $Tris_2GTP$ 0.3, phosphocreatine 14. In some experiments, EGTA was replaced by higher concentrations (10 or 30 mM) of the faster Ca^{2+} chelator BAPTA tetra-potassium salt. When 30 mM BAPTA was included, 0.69 mM or 5.7 mM Ca^{2+} was added to the internal solution to give 10 or 100 nM free [Ca^{2+}], respectively, at 33°C, pH 7.3 and overall ionic concentration 300 mM, according to the online program MAXCHELATOR, WEBMAXC EXTENDED version (https://somapp.ucdmc.ucdavis.edu/pharmacology/bers/maxchelator/webmaxc/webmaxcE.htm). The electrode resistance was 1-3 MΩ for somatic recordings and 3-5 MΩ for dendritic recordings. Series resistance was monitored throughout the recordings and was usually less than 20 MΩ; recordings were discarded when series resistance reached 25 MΩ or 30 MΩ, for somatic and dendritic recordings, respectively. Cells with resting membrane potentials depolarized beyond -60 mV at break-in were discarded.

NBQX (10 µM), DL-APV (50 µM), Gabazine (12.5 µM) and CGP55845 (1 µM) were applied in the external solution in all experiments to block glutamatergic and GABAergic neurotransmission, respectively, in order to isolate the contribution of the intrinsic ion channels to the ramp responses. Carbachol (2 µM), acetylcholine (2, 10, or 15 µM), flufenamic acid (100 µM), SKF96365 (50 µM), CBA (50 µM), and 9-phenanthrol (100 µM) were added to the external solution as needed, from stock solutions made with water, DMSO, or ethanol; the concentration of ethanol or DMSO in the final solution was ≤ 0.1%. Carbachol, 9-phenanthrol, and CBA were purchased from Tocris, CGP55845 from Abcam (Cambridge, MA), DL-APV from HelloBio (Princeton, NJ), NBQX, Gabazine, and SKF96365 from Alomone Labs (Jerusalem, Israel), and acetylcholine, flufenamic acid, and K4-BAPTA from Sigma (St. Louis, MO).

In order to approximate the depolarizing input that place cells receive as an animal traverses the place field, ramp-shaped depolarizing current injections were applied via the recording electrode to CA1 pyramidal neurons at either the soma or the apical dendrite (150-250 μm from soma). Two second ramps (1 s up, 1 s down) and ten second ramps (5 s up, 5 s down) were applied to simulate different running speeds. Current amplitude was adjusted to evoke peak frequencies between 10 and 25 Hz, comparable to place cell firing as recorded *in vivo* (Hargreaves et al., 2007; Resnik et al., 2012; Bittner et al., 2015).

Experimental design and statistical analyses

Experimental data were recorded and analyzed with Igor Pro software (WaveMetrics). Left or rightward shifts in firing along the current ramp were quantified as an adaptation index, as previously described (Upchurch et al., 2022):

$$\frac{\#APs\ on\ up\text{-}ramp - \#APs\ on\ down\text{-}ramp}{\#APs\ on\ up\text{-}ramp + \#APs\ on\ down\text{-}ramp}$$

Positive values indicate firing predominantly on the up-ramp, while negative values indicate firing mostly on the down-ramp. An adaptation index of zero indicates symmetry in the number of action potentials on the up-ramp and the down-ramp. Plots of instantaneous frequency versus time (f/T) or current (f/I) use the time or current value at the midpoint of the interspike interval (ISI), respectively.

An n = 6-12 is required for a typical patch clamp electrophysiology experiment that has a difference in means of 1.3-2X and a standard deviation of 0.2-0.3 for $p = 0.05$ and a power of 0.9 (Cohen, 1977). Each experimental group in this study is made up of $n \geq 8$ recording sessions; the number of cells recorded for each experiment is indicated in the Results section. Recordings were from one cell per slice; typically, a maximum of three recordings were obtained for each animal.

Statistical analyses were performed in SPSS (IBM, RRID:SCR_002865), following the tutorials and software guide from Laerd Statistics (2015, https://statistics.laerd.com/). Comparisons were made in the same cell before and after pharmacological treatment; the summary plots for these data include individual points and means ± standard error of the mean. Parametric analyses (paired samples t-test and repeated-measures ANOVA) were used to compare treatments in the same neurons, since data were normally distributed as determined by the Shapiro-Wilk test for normality. Significant differences demonstrated by repeated measures ANOVA were followed up by post-hoc analysis using Bonferroni-corrected pair-wise comparisons. Differences were considered to be statistically significant when $p < 0.05$.

Computational Modeling

A multicompartmental CA1 pyramidal neuron model from our laboratory was used as a starting point (Upchurch et al., 2022). This model was based on the model in the study by (Poirazi et al., 2003a), with subsequent changes made in studies by (Shah et al., 2008), (Bianchi et al., 2012), and (Combe et al.,

2018). The model was created from a reconstructed morphology (Megías et al., 2001) with 144 compartments. The following currents were modeled using Ohmic drive and conductances in parallel with a membrane capacitance (C_M) : a Na^+ current (I_{Na}), L-type (I_{CaL}), R-type (I_{CaR}), and T-type (I_{CaT}) Ca^{2+} currents, two delayed rectifiers (I_{Kv1} and I_{Kv2}), an A-type K^+ current (I_A), an inward rectifying potassium current (I_{KIR}), a nonspecific Ca^{2+}-activated current (I_{CAN}), a hyperpolarization-activated mixed cationic h-current (I_h), and a leak current (I_L). All currents were as in the previous model except (I_{CAN}), which was added to the model. In the soma and apical dendrites, we kept the Markov model of the Na_V channel that we modified from (Balbi et al., 2017). This Markov model was tuned to replicate the distance-dependent long-term inactivation of $Na_V1.6$ found in the literature (Mickus et al., 1999) that causes spike frequency adaptation and the difference in half activation between the soma and dendrites supported by (Gasparini and Magee, 2002).The sevenfold gradient in the h-conductance supported by (Magee, 1998), sixfold gradient in A-type potassium channels supported by (Hoffman et al., 1997) and lower sodium conductance in the dendrites versus the soma (75% of somatic value) supported by (Gasparini and Migliore, 2015) were also retained. A spine factor, to account for the additional membrane area due a higher density of spines (Megías et al., 2001) was varied as described in (Upchurch et al., 2022), and a sigmoidal decrease in membrane and axial resistance was implemented to account for the decrease in input resistance along the apical dendrites (Magee, 1998; Poirazi et al., 2003b).

The calcium handling for the model was modified from (Ashhad and Narayanan, 2013). The model performs a Ca^{2+} material balance on four shells in each compartment, and incorporates radial and longitudinal diffusion ($D_{Ca}\nabla^2[Ca^{2+}]$), stationary and mobile Ca^{2+} buffers (R_{Buf}),, calcium leak through endoplasmic reticulum leak channels (J_{leak}), Ca^{2+} uptake from a sarcoplasmic/endoplasmic reticulum Ca^{2+} ATPase pump (J_{SERCA}), a plasma membrane extrusion pump (J_{Pump}), Ca^{2+} from voltage gated channels on the membrane (J_{VGCC}), and IP_3 mediated Ca^{2+} induced Ca^{2+} release, CICR (J_{IP3R}). Details on the implementation of diffusion, the buffers, calcium leak and the pumps are described in (Ashhad and Narayanan, 2013). The differential equation for cytosolic calcium is described below, where A is a gradient in IP_3 mediated CICR receptors, and B is a gradient in the density of leak and SERCA pumps.

$$\frac{\partial Ca^{2+}}{\partial t} = D_{Ca}\nabla^2[Ca^{2+}] + AJ_{IP3R} + B(J_{leak} - J_{SERCA}) + R_{Buf} + J_{VGCC} - J_{Pump}$$

The IP_3 mediated CICR depends on the level of IP_3 and Ca^{2+} concentration and is characterized by:

$$J_{IP_3R} = J_{IP_3\mathrm{R\,max}}\left(\left(\frac{[IP_3]}{[IP_3] + K_{IP_3}}\right)\left(\frac{(Ca^{2+})}{Ca^{2+} + K_{act}}\right)h\right)^{\mathbf{3}} x\left(1 - \frac{(Ca^{2+})}{[Ca^{2+}]_{ER}}\right) mM\ ms^{-1}$$

Where $J_{IP3Rmax}$ is the maximum rate of IP_3 mediated CICR, 3500 μM s^{-1} and K_{IP3} is the disassociation constant for IP_3 binding the IP_3 receptor, 0.8 μM. The concentration of IP_3 was assumed to be at a steady

state of 0.16 μM in control conditions and 10 μM during simulations of carbachol application. $[Ca^{2+}]_{ER}$ is the Ca^{2+} concentration within the endoplasmic reticulum, 400 μM. K_{act} is the dissociation constant for Ca^{2+} binding onto the IP_3R activation site, 0.7 μM. The likelihood that Ca^{2+} is not bound to the inhibition site, h, is described by:

$$\frac{\mathrm{d}h}{\mathrm{d}r} = k_{on}(K_{\mathrm{inh}} - ([\mathrm{C}a^{2+}] + K_{\mathrm{inh}})h).$$

Where k_{on} is the rate of Ca^{2+} binding to the inhibition site and K_{inh} is the dissociation constant for calcium binding to the inhibition site. This produces the bell-shaped curve for the Ca^{2+} dependence as shown in the literature (Bezprozvanny et al., 1991; Fink et al., 2000), in which high levels of intracellular Ca^{2+} inhibit CICR. We modified the bell-shaped curve from (Bezprozvanny et al., 1991) by shifting the Ca^{2+} dependence to the right with a K_{act} of 0.7 μM and a K_{inh} of 0.6 μM as we did not expect the channel to be constitutively active at the estimated resting concentration of Ca^{2+} in the cell, 50 nM. The rate of increase of Ca^{2+} concentration due to IP_3R activation was based on the model calibrated by (Fink et al., 2000) and implemented in NEURON by (Ashhad and Narayanan, 2013). The cytoplasmic mouth of the IP_3R in the ER and cytosolic mouth of the TRPM4 in the plasma membrane were assumed to be co-localized (Gonzales and Earley, 2012; Provence et al., 2017), creating a nanodomain in which transiently high values of Ca^{2+} are achieved. We implemented the nanodomain by increasing the rate of increase of Ca^{2+} concentration fivefold in the nanodomain compared to that used in the rest of the model and allowing the nanodomain concentration to relax to the concentration of the outermost shell of the model with a time constant of 80 ms, with no other sources or sinks for Ca^{2+} in the nanodomain. As we assumed each nanodomain was paired with an individual IP_3 receptor, we did not include the gradient α in IP_3 receptors in accounting for Ca^{2+} in the nanodomain.

$$\frac{dCa_{ND}^{2+}}{dt} = 5 * J_{InsP3R} + \frac{Ca_{bulk}^{2+} - Ca_{ND}^{2+}}{80ms}$$

The TRPM4 model was modified from (Nilius et al., 2004) and assumes that the required binding of Ca^{2+} to the channel precedes voltage-dependent channel activation. The model has three different states, an unbound state, a Ca^{2+} bound closed state, and an open state.

$$TRPM4 \Leftrightarrow TRPM4\ bound\ to\ Ca^{2+} \underset{\alpha(V),\beta(V)}{\Longleftrightarrow} Open\ TRPM4\ channel$$

Ca^{2+} binding is assumed to be much faster than the voltage dependent gating and is assumed to instantaneously reach the steady state binding determined by the dissociation constant K_d (87 μM). The fraction of open channels *m* relaxes to the steady state activation m_∞ with a time constant, τ, with first order kinetics:

$$\alpha' = \frac{\alpha}{1+{Kd}/{[Ca^{2+}]_{ND}}}, m_\infty = \frac{\alpha'}{\alpha'+\beta} \qquad \tau = \frac{1}{\alpha'+\beta}$$

where α is the forward rate of Ca^{2+} bound TRPM4 opening, α(V) = 0.0057 exp(0.0060 V), α' is the forward rate scaled by the fraction of Ca^{2+} bound channels, β is the backward rate of TRPM4 closing, β(V) = 0.033 exp(−0.019 V) and $[Ca^{2+}]_{ND}$ is the Ca^{2+} concentration in the nanodomain coupled to IP_3 mediated CICR. To simulate the control and carbachol application experiments we assumed a change in the steady state concentration of IP_3. We injected enough current into the model to hold the membrane potential at -60 mV long enough for all transients to equilibrate before injecting a two second temporally symmetric current ramp either in the soma or 219 μm from the soma in the apical dendrites. The amplitude of the ramp was adjusted to reach similar peak frequencies as in the experiments, 10 to 25 Hz. As in the experiments, less current was needed to achieve higher frequencies in the simulations with high IP_3 concentration that model the effects of cholinergic receptor activation.

REFERENCES

Abbott LF, Blum KI (1996) Functional significance of long-term potentiation for sequence learning and prediction. Cereb Cortex N Y N 1991 6:406–416.

Acquas E, Wilson C, Fibiger HC (1996) Conditioned and unconditioned stimuli increase frontal cortical and hippocampal acetylcholine release: effects of novelty, habituation, and fear. J Neurosci Off J Soc Neurosci 16:3089–3096.

Arboit A, Reboreda A, Yoshida M (2020) Involvement of TRPC4 and 5 Channels in Persistent Firing in Hippocampal CA1 Pyramidal Cells. Cells 9.

Ashhad S, Narayanan R (2013) Quantitative interactions between the A-type K^+ current and inositol trisphosphate receptors regulate intraneuronal Ca^{2+} waves and synaptic plasticity: Transient K^+ current regulates ER Ca^{2+} release. J Physiol 591:1645–1669.

Autzen HE, Myasnikov AG, Campbell MG, Asarnow D, Julius D, Cheng Y (2018) Structure of the human TRPM4 ion channel in a lipid nanodisc. Science 359:228–232.

Avignone E, Cherubini E (1999) Muscarinic receptor modulation of GABA-mediated giant depolarizing potentials in the neonatal rat hippocampus. J Physiol 518:97–107.

Aznavour N, Mechawar N, Descarries L (2002) Comparative analysis of cholinergic innervation in the dorsal hippocampus of adult mouse and rat: A quantitative immunocytochemical study. Hippocampus 12:206–217.

Azouz R, Jensen MS, Yaari Y (1994) Muscarinic Modulation of Intrinsic Burst Firing in Rat Hippocampal Neurons. Eur J Neurosci 6:961–966.

Balbi P, Massobrio P, Hellgren Kotaleski J (2017) A single Markov-type kinetic model accounting for the macroscopic currents of all human voltage-gated sodium channel isoforms Gillespie D, ed. PLOS Comput Biol 13:e1005737.

Benardo LS, Prince DA (1982) Cholinergic excitation of mammalian hippocampal pyramidal cells. Brain Res 249:315–331.

Berridge MJ (1998) Neuronal Calcium Signaling. Neuron 21:13–26.

Bezprozvanny I, Watras J, Ehrlich BE (1991) Bell-shaped calcium-response curves of Ins(1,4,5)P3- and calcium-gated channels from endoplasmic reticulum of cerebellum. Nature 351:751–754.

Bianchi D, Marasco A, Limongiello A, Marchetti C, Marie H, Tirozzi B, Migliore M (2012) On the mechanisms underlying the depolarization block in the spiking dynamics of CA1 pyramidal neurons. J Comput Neurosci 33:207–225.

Bianchi L, Ballini C, Colivicchi MA, Della Corte L, Giovannini MG, Pepeu G (2003) Investigation on Acetylcholine, Aspartate, Glutamate and GABA Extracellular Levels from Ventral Hippocampus During Repeated Exploratory Activity in the Rat. Neurochem Res 28:565–573.

Bittner KC, Grienberger C, Vaidya SP, Milstein AD, Macklin JJ, Suh J, Tonegawa S, Magee JC (2015) Conjunctive input processing drives feature selectivity in hippocampal CA1 neurons. Nat Neurosci 18:1133–1142.

Bittner KC, Milstein AD, Grienberger C, Romani S, Magee JC (2017) Behavioral time scale synaptic plasticity underlies CA1 place fields. Science 357:1033–1036.

Bland BH, Colom LV, Konopacki J, Roth SH (1988) Intracellular records of carbachol-induced theta rhythm in hippocampal slices. Brain Res 447:364–368.

Blum KI, Abbott LF (1996) A model of spatial map formation in the hippocampus of the rat. Neural Comput 8:85–93.

Brown DA, Adams PR (1980) Muscarinic suppression of a novel voltage-sensitive K+ current in a vertebrate neurone. Nature 283:673–676.

Buchanan KA, Petrovic MM, Chamberlain SEL, Marrion NV, Mellor JR (2010) Facilitation of long-term potentiation by muscarinic M(1) receptors is mediated by inhibition of SK channels. Neuron 68:948–963.

Burke SN, Maurer AP, Yang Z, Navratilova Z, Barnes CA (2008) Glutamate receptor-mediated restoration of experience-dependent place field expansion plasticity in aged rats. Behav Neurosci 122:535–548.

Chen S, Benninger F, Yaari Y (2014) Role of small conductance Ca^{2+}-activated K^{+} channels in controlling CA1 pyramidal cell excitability. J Neurosci Off J Soc Neurosci 34:8219–8230.

Cohen J (1977) CHAPTER 1 - The Concepts of Power Analysis. In: Statistical Power Analysis for the Behavioral Sciences (Revised Edition), pp 1–17. Academic Press. Available at: https://www.sciencedirect.com/science/article/pii/B9780121790608500062 [Accessed January 11, 2018].

Colino A, Halliwell JV (1993) Carbachol Potentiates Q Current and Activates a Calcium-dependent Non-specific Conductance in Rat Hippocampus In Vitro. Eur J Neurosci 5:1198–1209.

Combe CL, Canavier CC, Gasparini S (2018) Intrinsic Mechanisms of Frequency Selectivity in the Proximal Dendrites of CA1 Pyramidal Neurons. J Neurosci 38:8110–8127.

Dani JA, Bertrand D (2007) Nicotinic Acetylcholine Receptors and Nicotinic Cholinergic Mechanisms of the Central Nervous System. Annu Rev Pharmacol Toxicol 47:699–729.

Dannenberg H, Young K, Hasselmo M (2017) Modulation of Hippocampal Circuits by Muscarinic and Nicotinic Receptors. Front Neural Circuits 11 Available at: https://www.frontiersin.org/articles/10.3389/fncir.2017.00102 [Accessed July 29, 2022].

Dasari S, Gulledge AT (2011) M1 and M4 receptors modulate hippocampal pyramidal neurons. J Neurophysiol 105:779–792.

Dienes C, Hézső T, Kiss DZ, Baranyai D, Kovács ZM, Szabó L, Magyar J, Bányász T, Nánási PP, Horváth B, Gönczi M, Szentandrássy N (2021) Electrophysiological Effects of the Transient Receptor Potential Melastatin 4 Channel Inhibitor (4-Chloro-2-(2-chlorophenoxy)acetamido) Benzoic Acid (CBA) in Canine Left Ventricular Cardiomyocytes. Int J Mol Sci 22:9499.

Disney AA, Higley MJ (2020) Diverse Spatiotemporal Scales of Cholinergic Signaling in the Neocortex. J Neurosci 40:720–725.

Dong C, Madar AD, Sheffield MEJ (2021) Distinct place cell dynamics in CA1 and CA3 encode experience in new environments. Nat Commun 12:2977.

Dutar P, Bassant MH, Senut MC, Lamour Y (1995) The septohippocampal pathway: structure and function of a central cholinergic system. Physiol Rev 75:393–427.

Dutta Banik D, Martin LE, Freichel M, Torregrossa A-M, Medler KF (2018) TRPM4 and TRPM5 are both required for normal signaling in taste receptor cells. Proc Natl Acad Sci 115 Available at: https://pnas.org/doi/full/10.1073/pnas.1718802115 [Accessed August 5, 2022].

Easton A, Douchamps V, Eacott M, Lever C (2012) A specific role for septohippocampal acetylcholine in memory? Neuropsychologia 50:3156–3168.

Egorov AV, Hamam BN, Fransén E, Hasselmo ME, Alonso AA (2002) Graded persistent activity in entorhinal cortex neurons. Nature 420:173–178.

Egorov AV, Schumacher D, Medert R, Birnbaumer L, Freichel M, Draguhn A (2019) TRPC channels are not required for graded persistent activity in entorhinal cortex neurons. Hippocampus 29:1038–1048.

Ekstrom AD, Meltzer J, McNaughton BL, Barnes CA (2001) NMDA Receptor Antagonism Blocks Experience-Dependent Expansion of Hippocampal “Place Fields.” Neuron 31:631–638.

Epsztein J, Brecht M, Lee AK (2011) Intracellular Determinants of Hippocampal CA1 Place and Silent Cell Activity in a Novel Environment. Neuron 70:109–120.

Fakler B, Adelman JP (2008) Control of K(Ca) channels by calcium nano/microdomains. Neuron 59:873–881.

Fernández de Sevilla D, Núñez A, Buño W (2021) Muscarinic Receptors, from Synaptic Plasticity to its Role in Network Activity. Neuroscience 456:60–70.

Fernandez FR, White JA (2010) Gain Control in CA1 Pyramidal Cells Using Changes in Somatic Conductance. J Neurosci 30:230–241.

Fink CC, Slepchenko B, Moraru II, Watras J, Schaff JC, Loew LM (2000) An image-based model of calcium waves in differentiated neuroblastoma cells. Biophys J 79:163–183.

Fisahn A, Pike FG, Buhl EH, Paulsen O (1998) Cholinergic induction of network oscillations at 40 Hz in the hippocampus in vitro. Nature 394:186–189.

Frank D, Kafkas A (2021) Expectation-driven novelty effects in episodic memory. Neurobiol Learn Mem 183:107466.

Fraser DD, MacVicar BA (1996) Cholinergic-Dependent Plateau Potential in Hippocampal CA1 Pyramidal Neurons. J Neurosci 16:4113–4128.

Gasparini S, Magee JC (2002) Phosphorylation-dependent differences in the activation properties of distal and proximal dendritic Na+ channels in rat CA1 hippocampal neurons. J Physiol 541:665–672.

Gasparini S, Migliore M (2015) Action Potential Backpropagation. In: Encyclopedia of Computational Neuroscience (Jaeger D, Jung R, eds), pp 133–137. New York, NY: Springer. Available at: https://doi.org/10.1007/978-1-4614-6675-8_123 [Accessed August 18, 2021].

Giessel AJ, Sabatini BL (2010) M1 Muscarinic Receptors Boost Synaptic Potentials and Calcium Influx in Dendritic Spines by Inhibiting Postsynaptic SK Channels. Neuron 68:936–947.

Giovannini MG, Rakovska A, Benton RS, Pazzagli M, Bianchi L, Pepeu G (2001) Effects of novelty and habituation on acetylcholine, GABA, and glutamate release from the frontal cortex and hippocampus of freely moving rats. Neuroscience 106:43–53.

Gómez-Ocádiz R, Trippa M, Zhang C-L, Posani L, Cocco S, Monasson R, Schmidt-Hieber C (2022) A synaptic signal for novelty processing in the hippocampus. Nat Commun 13.

Gonzales AL, Amberg GC, Earley S (2010) Ca^{2+} release from the sarcoplasmic reticulum is required for sustained TRPM4 activity in cerebral artery smooth muscle cells. Am J Physiol-Cell Physiol 299:C279–C288.

Gonzales AL, Earley S (2012) Endogenous cytosolic Ca2+ buffering is necessary for TRPM4 activity in cerebral artery smooth muscle cells. Cell Calcium 51:82–93.

Gu N, Vervaeke K, Hu H, Storm JF (2005) Kv7/KCNQ/M and HCN/h, but not K_{Ca} 2/SK channels, contribute to the somatic medium after-hyperpolarization and excitability control in CA1 hippocampal pyramidal cells: M- and h-channel functions in hippocampal pyramidal cells. J Physiol 566:689–715.

Guinamard R, Demion M, Launay P (2010) Physiological Roles of the TRPM4 Channel Extracted from Background Currents. Physiology 25:155–164.

Guinamard R, Simard C, Del Negro C (2013) Flufenamic acid as an ion channel modulator. Pharmacol Ther 138:272–284.

Hargreaves EL, Yoganarasimha D, Knierim JJ (2007) Cohesiveness of spatial and directional representations recorded from neural ensembles in the anterior thalamus, parasubiculum, medial entorhinal cortex, and hippocampus. Hippocampus 17:826–841.

Harney SC, Rowan M, Anwyl R (2006) Long-Term Depression of NMDA Receptor-Mediated Synaptic Transmission Is Dependent on Activation of Metabotropic Glutamate Receptors and Is Altered to Long-Term Potentiation by Low Intracellular Calcium Buffering. J Neurosci 26:1128–1132.

Hasselmo ME (2006) The role of acetylcholine in learning and memory. Curr Opin Neurobiol 16:710–715.

Hoffman DA, Johnston D (1998) Downregulation of Transient K+ Channels in Dendrites of Hippocampal CA1 Pyramidal Neurons by Activation of PKA and PKC. J Neurosci 18:3521–3528.

Hoffman DA, Magee JC, Colbert CM, Johnston D (1997) K+ channel regulation of signal propagation in dendrites of hippocampal pyramidal neurons. Nature 387:869–875.

Hofmann T, Obukhov AG, Schaefer M, Harteneck C, Gudermann T, Schultz G (1999) Direct activation of human TRPC6 and TRPC3 channels by diacylglycerol. Nature 397:259–263.

Hou J, Fei Y, Li W, Chen Y, Wang Q, Xiao Y, Wang Y, Li Y (2018) The transient receptor potential melastatin 4 channel inhibitor 9-phenanthrol modulates cardiac sodium channel: 9-Phenanthrol inhibits cardiac sodium channel. Br J Pharmacol 175:4325–4337.

Huerta PT, Lisman JE (1995) Bidirectional synaptic plasticity induced by a single burst during cholinergic theta oscillation in CA1 in vitro. Neuron 15:1053–1063.

Huff AE, McGraw SD, Winters BD (2022) Muscarinic (M1) cholinergic receptor activation within the dorsal hippocampus promotes destabilization of strongly encoded object location memories. Hippocampus 32:55–66.

Hutchison IC, Rathore S (2015) The role of REM sleep theta activity in emotional memory. Front Psychol 6 Available at: http://journal.frontiersin.org/article/10.3389/fpsyg.2015.01439 [Accessed August 26, 2022].

Knauer B, Jochems A, Valero-Aracama MJ, Yoshida M (2013) Long-lasting intrinsic persistent firing in rat CA1 pyramidal cells: A possible mechanism for active maintenance of memory: Long-Lasting Persistent Firing in Ca1 Pyramidal Cells. Hippocampus 23:820–831.

Kopsick JD, Hartzell K, Lazaro H, Nambiar P, Hasselmo ME, Dannenberg H (2022) Temporal dynamics of cholinergic activity in the septo-hippocampal system. Front Neural Circuits 16:957441.

Launay P, Fleig A, Perraud A-L, Scharenberg AM, Penner R, Kinet J-P (2002) TRPM4 Is a Ca2+-Activated Nonselective Cation Channel Mediating Cell Membrane Depolarization. Cell 109:397–407.

Lee I, Griffin AL, Zilli EA, Eichenbaum H, Hasselmo ME (2006) Gradual translocation of spatial correlates of neuronal firing in the hippocampus toward prospective reward locations. Neuron 51:639–650.

Lei Y-T, Thuault SJ, Launay P, Margolskee RF, Kandel ER, Siegelbaum SA (2014) Differential contribution of TRPM4 and TRPM5 nonselective cation channels to the slow afterdepolarization in mouse prefrontal cortex neurons. Front Cell Neurosci 8 Available at: http://journal.frontiersin.org/article/10.3389/fncel.2014.00267/abstract [Accessed August 25, 2022].

Levey A, Edmunds S, Koliatsos V, Wiley R, Heilman C (1995) Expression of m1-m4 muscarinic acetylcholine receptor proteins in rat hippocampus and regulation by cholinergic innervation. J Neurosci 15:4077–4092.

Li K, Abbott SBG, Shi Y, Eggan P, Gonye EC, Bayliss DA (2021) TRPM4 mediates a subthreshold membrane potential oscillation in respiratory chemoreceptor neurons that drives pacemaker firing and breathing. Cell Rep 34:108714.

Lin EC, Combe CL, Gasparini S (2017) Differential Contribution of Ca2+-Dependent Mechanisms to Hyperexcitability in Layer V Neurons of the Medial Entorhinal Cortex. Front Cell Neurosci 11:182.

Magee JC (1998) Dendritic Hyperpolarization-Activated Currents Modify the Integrative Properties of Hippocampal CA1 Pyramidal Neurons. J Neurosci 18:7613–7624.

Martina M, Schultz JH, Ehmke H, Monyer H, Jonas P (1998) Functional and Molecular Differences between Voltage-Gated K^+ Channels of Fast-Spiking Interneurons and Pyramidal Neurons of Rat Hippocampus. J Neurosci 18:8111–8125.

Masoli S, Tognolina M, Laforenza U, Moccia F, D'Angelo E (2020) Parameter tuning differentiates granule cell subtypes enriching transmission properties at the cerebellum input stage. Commun Biol 3:222.

Mederos Y Schnitzler M, Gudermann T, Storch U (2018) Emerging Roles of Diacylglycerol-Sensitive TRPC4/5 Channels. Cells 7.

Megías M, Emri Z, Freund TF, Gulyás AI (2001) Total number and distribution of inhibitory and excitatory synapses on hippocampal CA1 pyramidal cells. Neuroscience 102:527–540.

Mehta MR, Barnes CA, McNaughton BL (1997) Experience-dependent, asymmetric expansion of hippocampal place fields. Proc Natl Acad Sci 94:8918–8921.

Mehta MR, Quirk MC, Wilson MA (2000) Experience-Dependent Asymmetric Shape of Hippocampal Receptive Fields. Neuron 25:707–715.

Menigoz A, Ahmed T, Sabanov V, Philippaert K, Pinto S, Kerselaers S, Segal A, Freichel M, Voets T, Nilius B, Vennekens R, Balschun D (2016) TRPM4-dependent post-synaptic depolarization is essential for the induction of NMDA receptor-dependent LTP in CA1 hippocampal neurons. Pflüg Arch - Eur J Physiol 468:593–607.

Micheau J, Marighetto A (2011) Acetylcholine and memory: A long, complex and chaotic but still living relationship. Behav Brain Res 221:424–429.

Mickus T, Jung H, Spruston N (1999) Properties of Slow, Cumulative Sodium Channel Inactivation in Rat Hippocampal CA1 Pyramidal Neurons. Biophys J 76:846–860.

Mironov SL (2008) Metabotropic glutamate receptors activate dendritic calcium waves and TRPM channels which drive rhythmic respiratory patterns in mice: mGluR, TRPM4 channels, calcium waves and inspiratory bursts. J Physiol 586:2277–2291.

Nilius B, Mahieu F, Prenen J, Janssens A, Owsianik G, Vennekens R, Voets T (2006) The Ca2+-activated cation channel TRPM4 is regulated by phosphatidylinositol 4,5-biphosphate. EMBO J 25:467–478.

Nilius B, Prenen J, Droogmans G, Voets T, Vennekens R, Freichel M, Wissenbach U, Flockerzi V (2003) Voltage dependence of the Ca2+-activated cation channel TRPM4. J Biol Chem 278:30813–30820.

Nilius B, Prenen J, Janssens A, Voets T, Droogmans G (2004) Decavanadate modulates gating of TRPM4 cation channels: Decavanadate modulates TRPM4. J Physiol 560:753–765.

Nilius B, Prenen J, Tang J, Wang C, Owsianik G, Janssens A, Voets T, Zhu MX (2005) Regulation of the Ca2+ Sensitivity of the Nonselective Cation Channel TRPM4*. J Biol Chem 280:6423–6433.

Nyakas C, Luiten PGM, Spencer DG, Traber J (1987) Detailed projection patterns of septal and diagonal band efferents to the hippocampus in the rat with emphasis on innervation of CA1 and dentate gyrus. Brain Res Bull 18:533–545.

O'Malley JJ, Seibt F, Chin J, Beierlein M (2020) TRPM4 Conductances in Thalamic Reticular Nucleus Neurons Generate Persistent Firing during Slow Oscillations. J Neurosci 40:4813–4823.

Otto JF (2006) A Spontaneous Mutation Involving Kcnq2 (Kv7.2) Reduces M-Current Density and Spike Frequency Adaptation in Mouse CA1 Neurons. J Neurosci 26:2053–2059.

Pace RW, Mackay DD, Feldman JL, Del Negro CA (2007) Inspiratory bursts in the preBötzinger complex depend on a calcium-activated non-specific cation current linked to glutamate receptors in neonatal mice: Inspiratory drive potential mechanisms in preBötC neurons. J Physiol 582:113–125.

Palacios-Filardo J, Mellor JR (2019) Neuromodulation of hippocampal long-term synaptic plasticity. Curr Opin Neurobiol 54:37–43.

Palacios-Filardo J, Udakis M, Brown GA, Tehan BG, Congreve MS, Nathan PJ, Brown AJH, Mellor JR (2021) Acetylcholine prioritises direct synaptic inputs from entorhinal cortex to CA1 by differential modulation of feedforward inhibitory circuits. Nat Commun 12:5475.

Partridge LD, Valenzuela CF (2000) Block of hippocampal CAN channels by flufenamate. Brain Res 867:143–148.

Pedarzani P, McCutcheon JE, Rogge G, Jensen BS, Christophersen P, Hougaard C, Strøbaek D, Stocker M (2005) Specific enhancement of SK channel activity selectively potentiates the afterhyperpolarizing current I(AHP) and modulates the firing properties of hippocampal pyramidal neurons. J Biol Chem 280:41404–41411.

Pepeu G, Giovannini MG (2004) Changes in Acetylcholine Extracellular Levels During Cognitive Processes: Table 1. Learn Mem 11:21–27.

Picardo MCD, Sugimura YK, Dorst KE, Kallurkar PS, Akins VT, Ma X, Teruyama R, Guinamard R, Kam K, Saha MS, Del Negro CA (2019) Trpm4 ion channels in pre-Bötzinger complex interneurons are essential for breathing motor pattern but not rhythm Dubuc R, ed. PLOS Biol 17:e2006094.

Poirazi P, Brannon T, Mel BW (2003a) Arithmetic of subthreshold synaptic summation in a model CA1 pyramidal cell. Neuron 37:977–987.

Poirazi P, Brannon T, Mel BW (2003b) Pyramidal Neuron as Two-Layer Neural Network. Neuron 37:989–999.

Power JM, Sah P (2008) Competition between Calcium-Activated K+ Channels Determines Cholinergic Action on Firing Properties of Basolateral Amygdala Projection Neurons. J Neurosci 28:3209–3220.

Priestley JB, Bowler JC, Rolotti SV, Fusi S, Losonczy A (2022) Signatures of rapid plasticity in hippocampal CA1 representations during novel experiences. Neuron 110:1978-1992.e6.

Provence A, Rovner ES, Petkov GV (2017) Regulation of transient receptor potential melastatin 4 channel by sarcoplasmic reticulum inositol trisphosphate receptors: Role in human detrusor smooth muscle function. Channels Austin Tex 11:459–466.

Putney JW (2005) Physiological mechanisms of TRPC activation. Pflüg Arch - Eur J Physiol 451:29–34.

Reboreda A, Jiménez-Díaz L, Navarro-López JD (2011) TRP Channels and Neural Persistent Activity. In: Transient Receptor Potential Channels (Islam MdS, ed), pp 595–613 Advances in Experimental Medicine and Biology. Dordrecht: Springer Netherlands. Available at: http://link.springer.com/10.1007/978-94-007-0265-3_32 [Accessed August 9, 2022].

Resnik E, McFarland JM, Sprengel R, Sakmann B, Mehta MR (2012) The effects of GluA1 deletion on the hippocampal population code for position. J Neurosci Off J Soc Neurosci 32:8952–8968.

Riquelme D, Cerda O, Leiva-Salcedo E (2021) TRPM4 Expression During Postnatal Developmental of Mouse CA1 Pyramidal Neurons. Front Neuroanat 15:643287.

Roth ED, Yu X, Rao G, Knierim JJ (2012) Functional Differences in the Backward Shifts of CA1 and CA3 Place Fields in Novel and Familiar Environments Gilestro GF, ed. PLoS ONE 7:e36035.

Sarter M, Lustig C (2020) Forebrain Cholinergic Signaling: Wired and Phasic, Not Tonic, and Causing Behavior. J Neurosci 40:712–719.

Shah MM, Migliore M, Valencia I, Cooper EC, Brown DA (2008) Functional significance of axonal Kv7 channels in hippocampal pyramidal neurons. Proc Natl Acad Sci 105:7869–7874.

Simard C, Sallé L, Rouet R, Guinamard R (2012) Transient receptor potential melastatin 4 inhibitor 9-phenanthrol abolishes arrhythmias induced by hypoxia and re-oxygenation in mouse ventricle: Anti-arrhythmic effect of 9-phenanthrol. Br J Pharmacol 165:2354–2364.

Stocker M, Krause M, Pedarzani P (1999) An apamin-sensitive Ca2+-activated K+ current in hippocampal pyramidal neurons. Proc Natl Acad Sci U S A 96:4662–4667.

Takács VT, Cserép C, Schlingloff D, Pósfai B, Szőnyi A, Sos KE, Környei Z, Dénes Á, Gulyás AI, Freund TF, Nyiri G (2018) Co-transmission of acetylcholine and GABA regulates hippocampal states. Nat Commun 9:2848.

Thiel CM, Huston JP, Schwarting RKW (1998) Hippocampal acetylcholine and habituation learning. Neuroscience 85:1253–1262.

Upchurch CM, Combe CL, Knowlton CJ, Rousseau VG, Gasparini S, Canavier CC (2022) Long-Term Inactivation of Sodium Channels as a Mechanism of Adaptation in CA1 Pyramidal Neurons. J Neurosci 42:3768–3782.

Venkatesan K, Liu Y, Goldfarb M (2014) Fast-Onset Long-Term Open-State Block of Sodium Channels by A-type FHFs Mediates Classical Spike Accommodation in Hippocampal Pyramidal Neurons. J Neurosci 34:16126–16139.

Veress R, Baranyai D, Hegyi B, Kistamás K, Dienes C, Magyar J, Bányász T, Nánási PP, Szentandrássy N, Horváth B (2018) Transient receptor potential melastatin 4 channel inhibitor 9-phenanthrol inhibits K^+ but not Ca^{2+} currents in canine ventricular myocytes. Can J Physiol Pharmacol 96:1022–1029.

Yamada-Hanff J, Bean BP (2013) Persistent sodium current drives conditional pacemaking in CA1 pyramidal neurons under muscarinic stimulation. J Neurosci 33:15011–15021.

Yamasaki M, Matsui M, Watanabe M (2010) Preferential Localization of Muscarinic M1 Receptor on Dendritic Shaft and Spine of Cortical Pyramidal Cells and Its Anatomical Evidence for Volume Transmission. J Neurosci 30:4408–4418.

Yoshida M, Knauer B, Jochems A (2012) Cholinergic modulation of the CAN current may adjust neural dynamics for active memory maintenance, spatial navigation and time-compressed replay. Front Neural Circuits 6 Available at: http://journal.frontiersin.org/article/10.3389/fncir.2012.00010/abstract [Accessed August 26, 2022].

Zhang Z, Reboreda A, Alonso A, Barker PA, Séguéla P (2011) TRPC channels underlie cholinergic plateau potentials and persistent activity in entorhinal cortex. Hippocampus 21:386–397.

Zhu MX (2005) Multiple roles of calmodulin and other Ca2+-binding proteins in the functional regulation of TRP channels. Pflüg Arch - Eur J Physiol 451:105–115.